HHS Public Access

Author manuscript

Nature. Author manuscript; available in PMC 2022 October 26.

Published in final edited form as:

Nature. 2021 July ; 595(7866): 266–271. doi:10.1038/s41586-021-03624-x.

Obesity accelerates hair thinning by stem cell-centric converging mechanism

Hironobu Morinaga[1], **Yasuaki Mohri**[1], **Marina Grachtchouk**[2], **Kyosuke Asakawa**[1], **Hiroyuki Matsumura**[1], **Motohiko Oshima**[3], **Naoya Takayama**[4], **Tomoki Kato**[1], **Yuriko Nishimori**[1], **Yuriko Sorimachi**[5], **Keiyo Takubo**[5], **Takayoshi Suganami**[6], **Atsushi Iwama**[3], **Yoichiro Iwakura**[7], **Andrzej A. Dlugosz**[2], **Emi K. Nishimura**[1,8,*]

[1]Department of Stem Cell Biology, Medical Research Institute, Tokyo Medical and Dental University, 1-5-45 Yushima, Bunkyo-ku, Tokyo, 113-8510, Japan.

[2]Department of Dermatology, University of Michigan Medical School, Ann Arbor, MI 48109, USA.

[3]Division of Stem Cell and Molecular Medicine, Center for Stem Cell Biology and Regenerative Medicine, The Institute of Medical Science, The University of Tokyo, Tokyo, Japan.

[4]Department of Regenerative Medicine, Graduate School of Medicine, Chiba University, Chiba, Japan.

[5]Department of Stem Cell Biology, Research Institute, National Center for Global Health and Medicine, Tokyo, Japan.

[6]Department of Molecular Medicine and Metabolism, Research Institute of Environmental Medicine, Nagoya University, Nagoya, Japan.

[7]Centre for Animal Disease Models, Research Institute for Biomedical Sciences, Tokyo University of Science, Chiba, Japan.

[8]Division of Aging and Regeneration, Institute of Medical Science, The University of Tokyo, 4-6-1 Shirokanedai, Minato-ku, Tokyo, 108-8639, Japan.

Abstract

Obesity, a worldwide epidemic, predisposes to many ageing-associated diseases, yet its exact impact on organ dysfunction is largely unknown[1]. Hair follicles, mini-epithelial organs that grow hair, miniaturize by ageing to cause hair loss through the depletion of hair follicle stem cells (HFSCs)[2]. Here, we report that obesity-induced stress such as by high-fat diet (HFD) feeding primarily targets HFSCs to accelerate hair thinning. Chronological gene expression analysis revealed that HFD feeding for four consecutive days directs activated HFSCs toward epidermal keratinization by generating excessive reactive oxygen species yet retains HFSC pools in young

[*]Correspondence and requests for materials should be addressed to Emi K. Nishimura. emikn@g.ecc.u-tokyo.ac.jp.

Author contributions H.M. performed the majority of experiments with support from Y.M., K.A., H. Matsumura, Y.N. T.S. T.K. and A.I. M.G. and A.A.D. prepared *Gli2ΔC* and *Gli2ΔN* mice. M.O., N.T., and A.I. performed and analyzed ATAC-seq, Y.I. prepared *IL-1Ra* KO and *IL-1α;IL-1β* KO mice. Y.S. and K.T helped to perform OCR assay. H.M. and E.K.N designed the study and wrote the manuscript.

Competing interests E.K.N. is an inventor on a patent application (in preparation) related to this manuscript, which will be filed by the Tokyo Medical and Dental University.

Supplementary Information is available for this paper.

mice. Integrative analysis with stem cell fate tracing, epigenetic analysis and reverse genetics revealed that further feeding of HFD subsequently induces lipid droplets and NF-κB activation within HFSCs via autocrine/paracrine IL-1R signaling. Those integrated factors converge on the profound inhibition of Sonic hedgehog (Shh) signal transduction in HFSCs, thereby further depleting lipid-laden HFSCs through their aberrant differentiation and inducing hair follicle miniaturization and eventual hair loss. Conversely, Shh activation by transgenes or compounds rescues HFD-induced hair loss. These data collectively demonstrate that stem cell inflammageing induced by obesity robustly represses organ regeneration signals to accelerate the mini-organ miniaturization, and suggests the importance of daily prevention of organ dysfunction.

Obesity predisposes to many ageing-associated diseases and is tightly associated with the human lifespan[3-5]. While many organs functionally and structurally decline with obesity and/or ageing, whether obesity and/or a high fat diet (HFD) directly impact organ function and regeneration, which cell populations are targeted and how it happens are still largely unknown in most organs[6,7]. Tissue stem cells underlie organ homeostasis and ageing[8-10]. Hair follicle stem cells (HFSCs) in the bulge region self-renew and produce differentiated progenies at the onset of the proliferating phase (anagen) for cyclical regeneration of hair shafts. An age-associated deficiency of COL17A1, a hemidesmosome component that anchors HFSCs to the basement membrane, causes the depletion of HFSCs through their epidermal differentiation, resulting in stem cell-centric “hair follicle ageing” that causes hair follicle miniaturization and hair thinning[2,11]. Although obesity has been shown to be a risk factor for androgenic alopecia (AGA) in humans[12], whether it specifically targets AGA or rather generally induces or accelerates hair loss has not been tested.

First, to determine whether a western diet, such as a HFD, accelerates hair loss/thinning, elderly male littermates of C57BL/6N (wild-type, wt) mice that had not shown obvious hair thinning were fed a HFD or a normal diet (ND) for a month. Those HFD-fed aged mice showed diffuse type hair thinning (Fig. 1a). Next, to examine the effects of obesity in hair follicles, wt male mice were fed a HFD or a ND from two months old to twelve months old. The HFD-fed mice also showed decreased numbers of hairs with shaggy appearance and that was more obvious after hair cycle induction by hair depilation (Fig. 1b). Furthermore, a few rounds of hair cycle induction in HFD-fed mice but not in ND-fed mice induced severe and irreversible hair loss (Fig. 1c, Extended Data Fig. 1a, Supplementary Fig. 2), indicating that cyclic hair regeneration is targeted by HFD-induced stress and accelerates hair thinning. We next analyzed genetically obese mice, chemically diabetic mice, wt mice fed a high sucrose diet, HFD-fed female mice, and HFD-fed male C57BL/6J mice. Genetic models of obesity (*db/db, Ay/+* and *ob/ob*) mice and HFD-fed C57BL/6J mice also showed severe hair loss at 6 months (Extended Data Fig. 1b-f) following four rounds of hair regeneration, while HFD-fed female mice showed hair loss at 8 months (Extended Data Fig. 1g). In contrast, streptozotocin (STZ)-treated diabetic mice or mice fed a high sucrose diet did not show hair loss (Extended Data Fig. 1h-k). These results indicated that obesity-induced metabolic stress accelerates hair loss.

To examine the overall structures of hair follicles in HFD-fed mice, we conducted whole mount staining analysis of COL17A1 and K14 to identify HFSCs in the bulge and basal

cells, respectively. The results showed that hair follicle bulges have disappeared in some hair follicles of HFD-fed mice with or without retention of relatively large sebaceous glands (Fig. 1d, Extended Data Fig. 1l). Genetically obese *ob/ob* mice and HFD-fed female mice also followed the same processes of HFSC depletion (Extended Data Fig. 1m-o). Importantly, the degree of hair loss was correlated with body weight in HFD-fed mice (Extended Data Fig. 1p). Zigzag hairs became thinner and shorter in HFD-fed mice than awl hairs (Extended Data Fig. 2a,b), indicating that the small type of hair follicles with lower numbers of HFSCs are affected more severely. Eventually, the dermis also became atrophic whereas the dermal adipose layer expanded in HFD-fed mice[13] (Extended Data Fig. 2c), similarly to aged skin[14]. The epidermal thickness was comparable in HFD-fed mice, suggesting that HFSCs are more sensitive to a HFD than epidermal stem cells (Extended Data Fig. 2c). Further, entry into anagen (growing phase) was precociously induced in HFD-fed mice. Strikingly, precocious entry into telogen (resting phase) with a shorter hair cycle duration was also found in those mice (Extended Data Fig. 2d-f), probably because of the altered surrounding microenvironment including expanded dermal adipocytes that control the hair cycle[15,16]. No obvious inflammatory cell infiltrations were histologically detectable (Extended Data Fig. 2e) and no conspicuous reduction of the capillary network or innervation was found around hair follicles in the skin of HFD-fed mice (Extended Data Fig. 2g,h). Those data collectively suggested that obesity robustly accelerates hair thinning mainly through HFSC depletion.

Next, to investigate the stem cell dynamics in HFD-induced hair loss, we tracked the fate of GFP^+ HFSCs after HFD feeding in *K15CrePR; Rosa-H2B-EGFP* mice. In ND-fed mice, GFP^+ HFSCs remained in the bulge providing their progeny to the cycling portion of hair follicles to grow a hair shaft through their downward contiguous localization[17]. In contrast, after three months of HFD feeding, GFP^+ HFSCs were reduced in the bulge and became contiguously localized in the upper portion including sebaceous glands and the junctional zone, and also in the epidermis (Fig. 1e,f). The HFSC progeny in the epidermis can be distinguished from the small number of GFP^+ resident basal cells (2.3%) that were labelled upon treatment with RU486 even without HFD-feeding (Extended Data Fig. 3a). Those data collectively indicate that HFD-fed metabolic stress induced the fate change of HFSCs into the lineages of the upper portion of hair follicles including sebaceous glands and epidermal keratinocytes which are also found in aged skin[2]. Importantly, the stem cell fate dynamics were specifically found at anagen when HFSCs are activated. The aberrant localization of those epidermally-committed HFSC progeny was detectable as the ectopic appearance of $K1^+$ differentiating cells above the bulge area even during the natural hair cycle as well as following depilation or chemical hair removal that does not induce any significant apoptosis in the skin (Extended Data Fig. 3b-h). Those results provide evidence that HFD-induced obesity collaborates with the cyclic activation of HFSCs to strikingly change the fate of those HFSCs and eliminate them.

To identify the pathway(s) responsible for HFD-induced fate switching of HFSCs, we performed microarray, RNA-seq and Assay for Transposase Accessible Chromatin with high-throughput Sequencing (ATAC-Seq) analysis of FACS-sorted HFSCs from HFD-fed or ND-fed mice and HFSCs from young and from aged mice. Microarray analysis showed that the mRNA expression level of *Col17a1*, a key gene regulating HFSC self-renewal and

ageing, was reduced in HFSCs of aged mice but not in HFD-fed mice (Extended Data Fig. 4a), suggesting the existence of distinct mechanisms that cause HFD-induced hair loss. A motif analysis of ATAC-Seq peaks revealed that chromatin accessibility of NFATc1 and MED-1, which have crucial roles in maintaining the quiescent state of HFSCs[18], was reduced in HFD-fed mice (Extended Data Fig. 4b). These data may epigenetically explain the premature anagen induction by the HFD. Microarray data showed that several different changes including profound reductions of the MAPK and Sonic Hedgehog (Shh) pathways were found in anagen HFSCs of HFD-fed mice (Fig. 2a). The reduced MAPK signaling elicited by the HFD might represent the dysfunction of a niche-derived FGF signal[19] that represses HFSC quiescence. To further explore responsible pathways, we performed RNA-seq analysis for anagen HFSCs from ND- or HFD-fed mice. Again, Shh pathways were found to be reduced in HFSCs by HFD-feeding (Extended Data Fig. 4c-e). qPCR analysis also demonstrated that the Shh pathway is inhibited in anagen HFSCs in HFD-fed mice (Fig. 2b), in *ob/ob* and in *db/db* mice (Extended Data Fig. 4f) but was not found in different types of alopecia such as in the alopecia areata model[20]. The significant reduction of Shh signaling that plays a crucial role both in development[21,22] and in cyclic regeneration of hair follicles[23] possibly explains the defective hair follicle regeneration by HFSCs in obese mice.

To examine whether the inhibition of Shh signaling by HFD feeding causes the fate change and the depletion of HFSCs, we analyzed *K15CrePR; Rosa-rtTA; TetO-Gli2ΔC* transgenic mice[24], where the Shh pathway is specifically and transiently inhibited by expression of the dominant negative form of GLI2 in HFSCs (Fig. 2c). Inhibition of Shh signaling for 1 week with the concomitant induction of the hair cycle caused a depletion of HFSCs, the miniaturization/loss of hair follicles and hair loss after one month (Fig. 2d,e, Extended Data Fig. 5a,b). Lineage tracing showed that GFP^+ cells became localized in the junctional zone, sebaceous glands and in the epidermal layer, similar to their localization in HFD-fed mice (Fig. 2f,g, Extended Data Fig. 5c,d). Our data revealed that Shh signaling is crucial for preventing HFSCs from their epidermal terminal differentiation and the inhibition of Shh signaling in HFSCs by the HFD robustly induces progressive hair follicle miniaturization and eventual hair loss.

To characterize the mechanism involved in the specific inhibition of Shh signaling we further searched for responsible changes in gene expression profiles. Firstly, we found that multiple inflammatory cytokine signaling pathways, including the IL-1R pathway, that naturally converge on NFκB activation are activated within HFSCs in HFD-fed mice (Fig. 3a, Extended Data Fig. 6a,b). qPCR results showed that *Il-1β* expression was increased in total epidermis of HFD-fed mice (Fig. 3b). Consistently, immunostaining of skin sections revealed that NFκB became localized within the nuclei of HFSCs in HFD-fed mice (Extended Data Fig. 6c). Increased expression of Il-1β was also found in *ob/ob* and in *db/db* mice (Extended Data Fig. 6d). Secondly, 8-oxoguanine, a marker of oxidative damage, was also increased in the HFSCs of HFD-fed mice (Fig. 3c, Extended Data Fig. 6e), which is consistent with the fact that reactive oxygen species (ROS) are generated during free fatty acid metabolism and are augmented by inflammatory cytokine signaling with obesity[25]. Thirdly, lipid droplets accumulate within HFSCs in mice with long-term exposure to a HFD but not in mice with short-term exposure (Fig. 3d,e, Extended Data Fig. 6f-h), which suggests that lipotoxicity occurs in HFSCs due to dyslipidemia. Those lipid-laden

GFP$^+$ cells divide and differentiate into corneocytes (squames) or into sebocytes that excrete sebum lipids through the follicular opening (Extended Data Fig. 6g,h). To determine the responsible factor(s) that inhibit Shh signaling, we treated keratinocytes from neonatal epidermis that contains growing hair germs[26] with a lipid mixture (LM), with inflammatory cytokines (IL-1β[27], IL6 and TNFα), or with H_2O_2. The results showed that treatment with IL-1β, IL6, LM or H_2O_2 inhibited the expression of Shh signal targets, including *Gli1, Gli2* and *Ptch1*, while treatment with TNFα did not (Fig. 3f, Extended Data Fig. 6i), which suggests that those inflammatory signaling factors and oxidative stress collectively repress the Shh signaling pathway in HFSCs. Local administration of IL-1β inhibited Shh signaling in anagen HFSCs of 7-week-old, 17-month-old and 22-month-old mice (Fig. 3g, Extended Data Fig. 6j). In contrast to old mice, *Cox2* expression was not increased by local administration of IL-1β in young mice, suggesting that there is a homeostatic mechanism that resists acute inflammatory signals in young animals. Furthermore, *IL-IRa* KO mice, in which the IL-1R pathway is constitutively activated[28], displayed partial hair thinning with some reduction of bulge number (p value = 0.0883) (Extended Data Fig. 6k-m and Supplementary Fig. 4). These data suggested that HFD-induced local activation of IL-1R signaling inhibits Shh signaling in HFSCs.

Next, we studied which types of cells secrete IL-1β to affect HFSCs in HFD-fed mice. The population of CD45$^+$ immune cells, especially CD3$^+$ T cells, was increased in the dermis of HFD-fed mice (Extended Data Fig. 7a-c), yet *IL-1β* expression was not significantly increased in those immune cells (Extended Data Fig. 7d). Instead, the expression of *IL-1β* in the total epidermis and in anagen HFSCs of HFD-fed mice was increased (Fig. 3b, Extended Data Fig. 7e). These data suggest that the HFD induces autocrine/paracrine IL-1R signaling to cause HFSC depletion in response to systemic lipid-induced stress.

We next searched for the early changes in HFSCs following HFD feeding in young mice. DCFDA and MitoSOX analyses showed that ROS generation both in whole cells and in mitochondria was increased in activated HFSCs within the first four days of HFD feeding (Extended Data Fig. 8a) followed by the later accumulation of 8-oxoguanine after 4 months of HFD feeding (Fig. 3c, Extended Data Fig. 8b). To determine how HFD feeding increases the accumulation of ROS, we measured the oxygen consumption rate (OCR) of enriched epidermal basal cells including HFSCs after the addition of fatty acids. The OCR of epidermal basal cells treated with a lipid mixture or with palmitate was significantly increased (Extended Data Fig. 8c). Further, the number and morphology of mitochondria showed no detectable changes in HFSCs by short-term HFD (Extended Data Fig. 8d). These data suggest that a HFD-derived nutrient shift increases ROS generation through aerobic respiration by fatty acids.

While the epidermal differentiation (keratinization) pathway was significantly upregulated by four days of HFD feeding, the overall gene expression changes were minimal and the inactivation of Shh signaling or the activation of the NFκB and IL-1R pathways were not detectable at such an early time point (Extended Data Fig. 8e,f). Short-term (three days) topical treatment of the skin with H_2O_2 significantly increased the appearance of K1$^+$ cells in the upper hair follicles but did not inhibit Shh signaling, suggesting that aberrant ROS

generation in HFSCs directly changed their fate into epidermal keratinocytes (Extended Data Fig. 8g,h).

To determine the most critical fate-determining step, we performed rescue experiments. *IL-1α, IL-1β* dKO mice[28], *TNFα* KO mice and/or wt mice treated with an antioxidant agent, α-lipoic acid[29], did not show any significant rescue effect (Extended Data Fig. 9a-d). Knockout of *Nrf2*, a key transcription factor that regulates the expression of antioxidant enzymes, did not accelerate hair loss with HFD feeding (Extended Data Fig. 9e). The forced expression of COL17A1 by HFSCs in *COL17A1* Tg mice, which delays/represses chronological hair follicle ageing[2], was not sufficient to rescue the HFD-induced hair loss (Extended Data Fig. 9f). Finally, we tested whether the activation of Shh signaling in HFSCs would rescue the hair loss. *K19CreER; Rosa-rtTA; TetO-Gli2ΔN* mice (*Gli2ΔN* mice), where Shh is specifically and transiently activated in HFSCs during treatment with doxycycline[30], partially rescued HFD-induced hair loss by promoting HFSC maintenance (Fig. 4a,b, Extended Data Fig. 9g). Similarly, pharmacological treatment with smoothened agonist (SAG), a small molecule that activates Shh signaling, also partially rescued the HFD-induced hair loss but not the aging-induced hair loss (Fig. 4c, Extended Data Fig. 9h-k). Taken together, these findings demonstrate that the Shh signaling deficiency in HFSCs caused by the HFD critically induced hair loss (shown schematically in Fig. 4d, Extended Data Fig. 10).

Because obesity needs multiple rounds of hair cycles to diminish HFSC pools, obesity is not just a risk factor for alopecia but could collaborate with repetitive hair cycle- or ageing-induced changes to profoundly abrogate HFSC self-renewal. The mechanism further reinforces the “stem cell-centric organ ageing theory”[2,11] based on human and mouse studies. Epidermal fate changes of HFSCs rarely occur during homeostasis in young animals but do occur during wound healing to transiently repair the epidermis[31], suggesting that stem cell inflammatory signals may similarly underlie the physiological processes. The data in this study were obtained using mice, which has limitations in humans yet proves the higher risk of alopecia with obesity. The strong and sharp impacts of diet and obesity on somatic stem cells suggest the importance of daily prevention of organ dysfunction by lifestyle management and could open new avenues for the treatment of common alopecia and other obesity/age-associated regeneration defects and diseases.

Methods

Mice

Animal care was in accordance with the guidance of the Tokyo Medical and Dental University for animal and recombinant DNA experiments. Mice were housed individually in cages at a maximum density of 5 mice per cage and kept on a 12-h light-dark cycle. The ambient temperature was maintained at 25° C with 40-80 % humidity. C57BL/6N and C57BL/6J mice were purchased from the Sankyo Labo Service. The following mouse cell lines were used: *K15CrePR*[31], *Rosa-H2B-EGFP* (Riken CDB), *Rosa-lsl-rtTA* (Jackson lab, #005670), *tetO-Gli2ΔC*[24] *IL-1Ra KO*[28] *K19CreER* (Riken BRC), *TNFα KO*[32], *Nrf2 KO*[33], *COL17A1* Tg[34] and *tetO-Gli2ΔN*[30]. More than 3 mice were used for each experiment. Hair depilation was conducted by plucking or by a hair removal cream (Epilat, Kracie) as

described in each Figure Legend. When using a hair removal cream, the dorsal skin was shaved and then treated with a hair removal cream for 3 min, after which the cream was washed off with warm water. *K15CrePR* induction was performed by topical application of 20 mg/ml Ru486 for 5 days on the dorsal skin of 7-week-old mice. GFP-positive cells were counted in telogen stage at the times indicated in the Figures. *K19CreER* induction was performed by an intraperitoneal injection of 100 μl 20 mg/ml tamoxifen for 5 days. The 60 kcal% HFD (D12492) and the doxycycline diet (D10001+0.0625% Doxycycline) were purchased from Research Diets. For treatment with α-lipoic acid, a HFD containing 2% w/w α-lipoic acid was used for four months during the HFD treatment[35]. For treatment with SAG, 100 μl 100 μM SAG (Calbiochem, 364590-63-6) in DMSO was applied using a Pipetman on the dorsal surface after hair depilation for 5 days.

Histology and immunofluorescence

Immunofluorescence was performed as described previously[2]. The following antibodies or chemical compounds were used: COL17A1 (Abcam, ab186415, 1:400), Keratin 14 (Biolegend, 906004, 1:500), ITGA6 (BD, 555734, 1:200), Keratin 15 (Biolegend, 833904, 1:300), NFκB (Santa Cruz, sc-101749, 1:50), CD11b (BD, 557686, 1:100), F4/80 (Bio-Rad, MCA497A488, 1:100), KI67 (Invitrogen, 14-5698-82, 1:300), CD3 (Biolegend, 100235, 1:100), MHC2 (Biolegend, 107605, 1:100), CD31(BD Biosciences, 557355, 1:200), anti-DNA/RNA Damage (Abcam, ab62623, 1:2000), Tom20 (Thermo Fisher, 11802-1-AP, 1:30), Keratin 1 (Abcam, ab185628, 1:300), survivin (Cell signaling, 2808, 1:100), casp3 (Cell signaling, 9661, 1:200), Tuj1 (Covance, PRB-435P, 1:500), CD34-FITC (Invitrogen, 11-0341-85, 1:100), ITGA6-PE (BD, 555736, 1:100), Sca1-APC (Miltenyi Biotec, 130-102-343, 1:100), CD45-APC-cy7 (BioLegend, 103116, 1:100). FV10-ASW4.2 was used for capturing confocal images. CellSens Standard v1.13 (Olympus) was used for collecting HE data.

Whole mount immunofluorescence

Whole mount staining of dorsal skin was performed as described previously with slight modifications[36]. Briefly, mouse skin was fixed with 4% paraformaldehyde (PFA) for 1 h on ice following by washing with 0.2% Tween 20/PBS, and subsequent blocking by PBSTM buffer (0.25% Fish skin gelatin, 1% skim milk, 0.5% Triton X-100 in PBS) for 1 h at room temperature (RT). Primary and secondary antibody reactions were performed in PBSTM buffer at 4°C overnight. After washing, skin samples were rendered transparent with BABB (benzyl alcohol mixed with benzyl benzoate at 1:2) as follows: Samples were dehydrated with 50% (vol/vol) methanol/PBS, rocked at RT for 10 min, then transferred to 100% methanol for 10 min at RT. After replacement of the methanol with 50% (vol/vol) BABB/methanol, samples were incubated for 5 min followed by the replacement of BABB/methanol with 100% BABB. Samples were then further incubated for 5 min. To obtain confocal images, samples were transferred to a slide glass with silicone grease to help hold the coverslips. To observe GFP by whole mount staining, the CUBIC transparent method was performed instead of BABB as follows: Briefly, after fixing with 4% PFA, samples were incubated with the 1st CUBIC buffer (25% urea, 25% N,N,N',N'-tetrakis(2-hydroxypropyl) ethylenediamine, 15 wt% Triton X-100) overnight at 4°C. After washing, the primary and secondary antibody reactions were performed at 4°C overnight or for 4 h, respectively. The

samples were then incubated with the 2nd CUBIC buffer (50% sucrose, 25% urea, 10% aminoalcohol, 0.1% (v/v) Triton X-100) overnight at 4°C.

Streptozotocin and glucose assessment

C57BL/6N 7-week-old male mice, each weighing 20–25 g, were purchased from Sankyo Labo Service. Obliteration of pancreatic β-cells was achieved with intraperitoneal injections of 50 mg/kg streptozotocin (STZ, Sigma-Aldrich) in 50 mmol/L sodium citrate buffer (pH 5) for 5 consecutive days. Seven days after the initial injection, mice with fasting blood glucose levels of 120 mg/dL after 18 h were deemed diabetic, and measurement of blood glucose levels were performed with terminal tail vein blood using a Breeze 2 (Bayer). A total of 9 diabetic mice were used in this experiment.

Single cell isolation from mouse dorsal skin

Single cells from mouse dorsal skin were obtained as described previously[37]. Briefly, dorsal skin was placed dermis side down in 0.25% trypsin (Gibco) or 0.2% Dispase II (Roche) for 12-14 h at 4°C. The epidermis and dermis were then obtained by scraping the skin gently. The epidermis was minced with a razor blade and then filtered with strainers (40 μm) (BD Falcon). The dermis was minced using scissors and the pieces were incubated in 0.2% collagenase (Sigma) for 1 h at 37°C with gentle agitation. Those suspensions were filtered with 70 μm strainers and epidermal and dermal cells were obtained after two washes with PBS.

FACS

Epidermal and dermal cell suspensions were incubated with the appropriate antibodies for 1 h at 4°C. Staining with 7-AAD (BD Bioscience) was used to exclude dead cells. Cell isolations were performed using a FACS AriaII or AriaIIIu equipped with Diva software version 6.1.3 (BD Bioscience). For RNA extraction of HFSCs, populations were sorted directly into Buffer RLT (Qiagen).

Microarray analysis

HFSCs ($CD34^{high}ITGA6^{high}SCA1^{-}$) were harvested from ND- and from HFD- fed mice after 3 months of treatment (each mouse is then 5 months old) using FACS. Repeated hair depilation was not performed for microarray analysis. Telogen HFSCs were isolated from telogen region and anagen HFSCs were obtained 3 days after hair depilation using hair plucking at the telogen region. FACS-sorted HFSCs were stored into Buffer RLT (Qiagen). 10,000 cells per sample were obtained from one mouse for telogen HFSCs and from four (ND) or eight (HFD) mice for anagen HFSCs. Microarray analysis was performed by the Chemicals Evaluation and Research Institute (CERI). All array data were deposited in the GEO public database (accession no. GSE131958).

RNA seq analysis

Anagen HFSCs were obtained 3 days after hair plucking at telogen region from ND- and from HFD-fed mice after 4 months treatment. 5,000 to 10,000 cells per sample were obtained from one mouse. Library preparation and sequencing analysis on an Illumina

NovaSeq 6000 was performed by GENEWIZ Inc. The expression of each gene derived from the read alignments was normalized to fragments per kilobase of exon model per million (FPKM) for further analysis. RNA-seq data were deposited in the GEO public database (accession no. GSE169173).

Assay for Transposase Accessible Chromatin with high-throughput (ATAC)-sequencing

FACS-sorted HFSCs (20,000 cells) or epidermal keratinocytes (ITGA6^{high} SCA1^{+}) were lysed in cold lysis buffer (10 mM Tris-HCl, pH 7.4, 10 mM NaCl, 3 mM $MgCl_2$, 0.1% IGEPAL CA-630) on ice for 10 min. After centrifugation, nuclei in the pellets were resuspended in 50 μl transposase reaction mix (25 μl Tagment DNA buffer (Illumina), 2.5 μl Tagment DNA enzyme (Illumina) and 22.5 μl water), incubated at 37°C for 35 min and then purified with a MinElute PCR Purification Kit (Qiagen). After optimization of PCR cycle numbers using SYBR GreenI Nucleic Acid gel Stain (Takara Bio), transposed fragments were amplified using NEBNext High Fidelity 2x PCR Master mix and index primers, and were purified with a MinElute PCR Purification Kit (Qiagen). Library DNAs were size-selected (240-360 bp) with BluePippin (Sage Science). Sequencing was performed using HiSeq1500 (Illumina) with a single-read sequencing length of 60 bp. Bowtie2 (version 2.2.6; with default parameters) was used to map reads to the reference genome (UCSC/mm10) with annotation data from iGenomes (Illumina). Reads mapped to mitochondria were removed. To ensure even processing, reads were randomly downsampled from each sample to adjust to the smallest read number of samples. MACS (version 2.1.1; with default parameters) was used to call peaks in the downsampled reads. The catalogue of all peaks called in all samples was produced by merging all called peaks that overlapped by at least one bp using bedtools. The MACS bdgcmp function was used to compute the fold enrichment over the background for all populations, and the bedtools map function was used to identify the maximum fold enrichment observed at each peak in the catalogue in each population. Maximum fold enrichment at each site in the catalogue was quantile normalized between samples using the PreprocessCore package in R (3.3.2). We used the Homer package with command annotatePeaks.pl using default parameters to annotate regions with promoter and distal labels and the nearest gene, and with command findMotifsGenome.pl using default parameters to identify enriched motifs, and the catalogue of all called peaks as a background.

DAVID functional enrichment analysis

To perform gene pathway analysis, we used the web-based Database for Annotation, Visualization and Integrated Discovery (DAVID). For analysis of anagen HFSCs, upregulated genes in the HFSCs of HFD-fed mice with a fold change ≥2 (Extended Data Fig. 8f) and downregulated genes with a fold change <0.5 (Fig. 2a) were used for BioCarta pathway enrichment analysis. For telogen HFSCs, upregulated genes in HFD-fed mice with a fold change >2.0 and $p<0.1$ were used for BioCarta pathway enrichment analysis (Fig. 3a). All pathways with $p<0.05$ are shown.

Gene set enrichment analysis (GSEA)

GSEA was provided by the Broad Institute of MIT and Harvard University. GSEA was used to investigate the potential mechanisms upregulated in telogen HFSCs or

downregulated in anagen HFSCs in HFD-fed mice using c2 (c2.cp.biocarta.v5.0.symbols or c2.cp.biocarta.v7.2.symbols, respectively) as the gene set correlation. All pathways with $p<0.1$ for upregulated in telogen HFSCs or those with $p<0.05$ for downregulated in anagen HFSCs were shown.

Real time qPCR

Total RNAs were purified from FACS-sorted cells by directly sorting into Buffer RLT (Qiagen) using a RNeasy micro Kit (Qiagen). cDNAs were then synthesized in 20 μl reaction mixtures using a High Capacity cDNA Reverse Transcription kit (Applied Biosystems) according to standard procedures. Quantitative PCR was performed using a SYBR Green qPCR Kit (Agilent Technology). Relative levels of expression were determined by normalization to β-actin using the ddCt method. The reactions were run in a Mx3000P Real-Time QPCR System (Agilent Technology). The primer sequences used were as follows: *β-actin*: 5′- GGCACCACACCTTCTACAATG-3′, 5′-GTGGTGGTGAAGCTGTAG-3′, *mKeratin1*: 5′-AGGATCTTGCCAGATTGCTG-3′, 5′-CTACTGCTTCCGCTCATGCT-3′, *mGli1*: 5’-GGTGCTGCCTATAGCCAGTGTCCTC-3’, 5’-GTGCCAATCCGGTGGAGTCAGACCC-3’, *mGli2*: 5’-TACCTCAACCCTGTGGATGC-3’, 5’-CTACCAGCGAGTTGGGAGAG-3’, *mPtch1*: 5’-ATCTCGAGACCAACGTGGAG-3’, 5’-TAGCGCCTTCTTCTTTTGGA-3’, *mIl-1b1*: 5’-GCAACTGTTCCTGAACTCA-3’, 5’-CTCGGAGCCTGTAGTGCAG-3’. *mIl-1b2*: 5’-CAACCAACAAGTGATATTCTCCATG-3‘, 5’-GATCCACACTCTCCAGCTGCA-3’. Uncropped gel images are shown in Supplementary Fig. 1.

IL-1β administration

Dorsal hairs of 7-week-old or 21-month-old male mice were depilated to induce anagen. Two days after depilation, an atelocollagen sponge (KOKEN, CSH-10) impregnated for 2 h at RT with 50 μl PBS or 1 μg recombinant IL-1β (Sigma, SRP-3083) was implanted subcutaneously in the dorsal skin of each mouse. The next day, HFSCs ($CD34^{high}$, $ITGA6^{high}$, $SCA1^{-}$) were collected by FACS following qPCR analysis.

DCFDA and MitoSOX assays

The oxidation-sensitive fluorescent probes 2′,7′-dichlorodihydrofluorescein diacetate (DCFDA, Invitrogen, D399) and MitoSOX Red (Invitrogen, M36008) were used to analyze the total intracellular content of ROS and mitochondrial superoxide production, respectively. Dorsal skin cells were harvested as described previously and incubated with 200 μM DCFDA or 20 μM MitoSOX Red with antibodies (CD34, ITGA6, SCA1) at 4°C for 60 min. Fluorescence was measured in the HFSC populations (singlet live cells, $CD34^{high}$, $ITGA6^{high}$, $SCA1^{-}$).

Immunostaining of 8-oxoguanine

8-Oxoguanine (8G) staining was performed as described previously[38,39]. Briefly, antigen retrieval was performed for 20 min at 95°C with citrate buffer (pH 6.0) on 4 μm paraffin sections. Sections were permeabilized for 20 min with 0.05% Triton X-100 in PBS, and were then blocked with 10% goat serum in PBS for 1 h at RT. The 1^{st} antibody (anti-

DNA/RNA Damage, ab62623, 1:2000) was incubated overnight at 4°C and the 2nd antibody (anti-mouse IgG, A21202 1:300) for 2 h at RT. Both reactions were performed in DAKO mounting medium (S3023).

Flux analyzer

The oxygen consumption rate (OCR) was measured using a Seahorse XF96 extracellular flux analyzer according to the manufacturer's instructions. Briefly, 1 x 10^5 cells from the total epidermis (many of which are basal keratinocytes) from 8 week old mice were transferred to a culture plate pre-coated with Cell-Tak containing SF-03 medium and centrifuged at 400 x g for 5 min. A 4% lipid mixture or 200 μM palmitate were added to the medium before measurement. The OCR was measured with sequential addition of 1 μM oligomycin, 2 μM FCCP, 0.5 μM rotenone/antimycin and 50 mM 2-deoxy-D-glucose.

Statistics

Statistical analyses were performed with GraphPad Prism 6 or 8 and Excel 2013. Two-tailed Student's t-test, two-tailed Mann–Whitney U-test, one-way ANOVA with two-tailed Dunnett's test or one-way ANOVA with two-tailed Tukey's test was used as described in the legend. P-values were adjusted for all multiple comparisons. DAVID pathway analysis used a modified Fisher's exact test to measure the significance of the gene-enrichment in annotation pathways. Image J version 1.51 was used for image analysis.

Extended Data

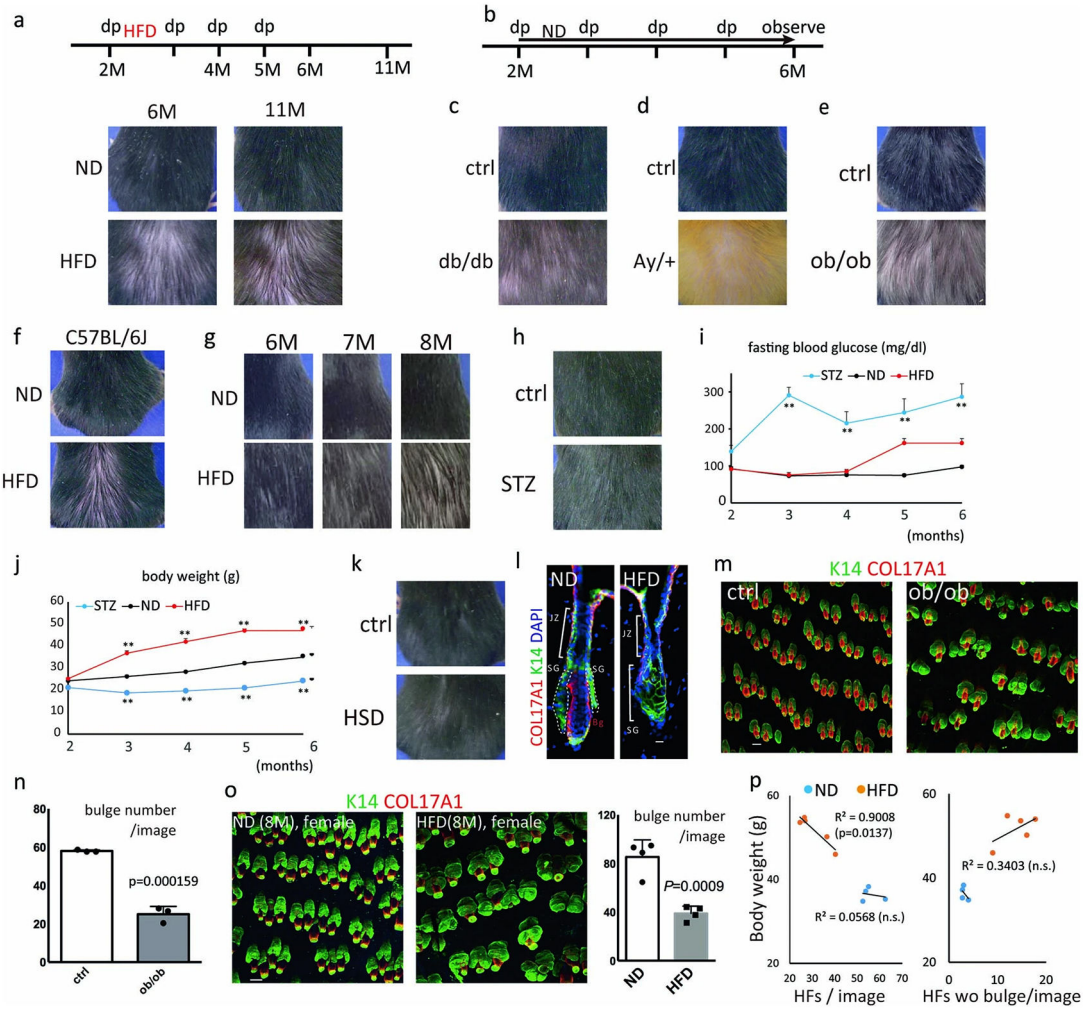

Extended Data Fig. 1 |. Obesity accelerates hair loss with repeated hair cycle induction.

a, Experimental design for **a, f, g**, and representative images of mice fed a ND or a HFD as indicated (n=4). **b**, Experimental design for **c-e, h. c-e**, Genetically obese mice were fed a ND with hair cycle induction at the indicated times and representative images are shown (n=4 each for control or obese mice). **f**, Representative images of C57BL/6J mice fed a ND or a HFD (n=3). **g**, Representative images of female mice fed a ND or a HFD (n=4). **h-j**, Representative images, fasting blood glucose levels and body weights of streptozocin-induced diabetic mice (ND, n=4, HFD, n=4, STZ-treated mice, n=8, two-tailed Dunnett's test, **, $p<0.05$; exact P values are provided in the Source Data. data are shown as means ± SD). **k**, Representative images of mice fed a ND or a high sucrose diet (HSD) (n=4). **l**, Representative cross-section images of hair follicles from three ND-fed or three HFD-fed mice. The bulge and basal layer was stained with COL17A1 and K14, respectively. JZ, junctional zone; SG, sebaceous gland; Bg, bulge. **m-o**, Whole mount images and bulge numbers of *ob/ob* mice (n=3, two-tailed unpaired t-test) or HFD-fed female mice (n=4, two-tailed unpaired t-test). Scale bar, 60 μm. **p**, Correlation between the degree of obesity

and hair follicle number or the number hair follicles without bulge (SG only) after five months treatment of HFD or ND with monthly hair depilation by plucking. Two-tailed Pearson's correlation coefficient. ns. not significant; wo, without. Data are shown as means ± SD.

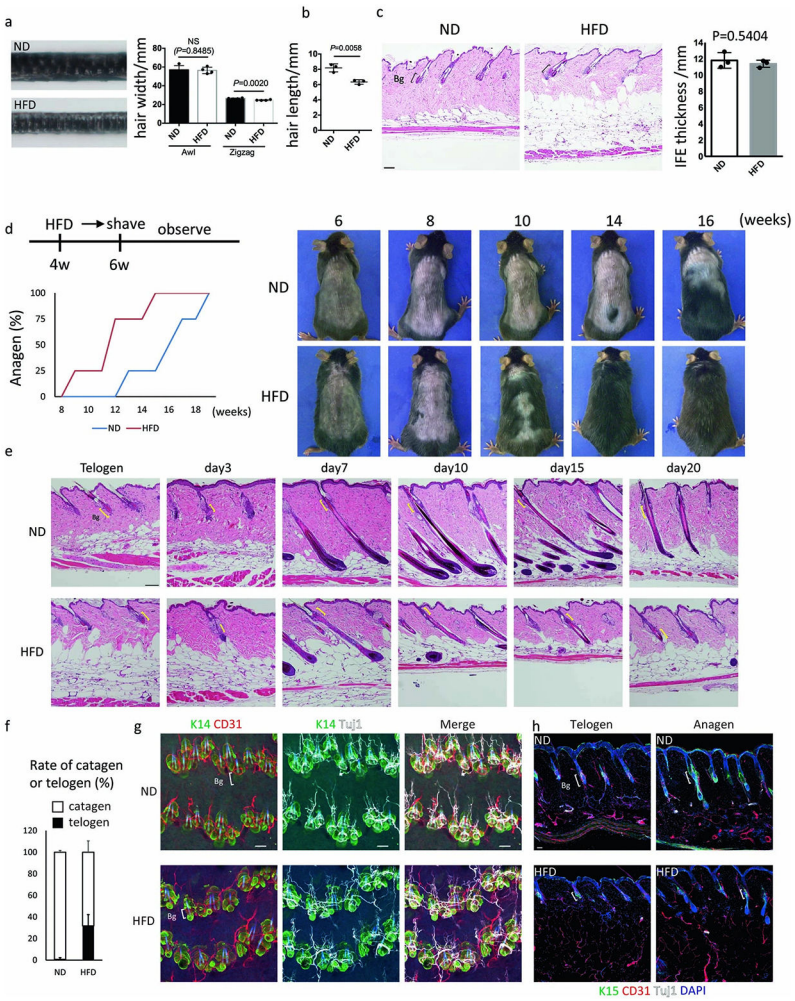

Extended Data Fig. 2 |. A HFD prematurely accelerates hair cycle progression.
a, The maximum hair diameters of zigzag and awl hairs in 6-month-old mice (4-months of treatment with a ND or a HFD). Images are representative zigzag hairs (n=4, two-tailed unpaired *t*-test. Data are shown as means ± SD). Awl, Awl hair; zigzag, zigzag hair. **b**, Length of hairs of 6-month-old mice (n=4, two-tailed unpaired *t*-test. Data are shown as means ± SD). **c**, HE staining and IFE thickness of the skin of ND- or HFD- fed 6-month-old mice (n=3, two-tailed unpaired t-test). Bg, bulge. Scale bar, 100 μm. **d**, Assay of anagen induction of HFD-fed mice; the HFD was started from 4 weeks old and hair was shaved at 6 weeks old. Anagen onset was judged by skin color change (n=4). **e**, HE staining of hair follicles from telogen to catagen of 5-month-old mice (3 months treatment with a ND or a HFD). Representative images from three mice at each hair stage are shown. Hair depilation by hair plucking was conducted at telogen and samples were observed at the indicated days after hair depilation. Scale bar, 100 μm. **f**, The rate of catagen or telogen hair follicles 20

days after anagen induction. **g, h**, Whole mount imaging (g) and section imaging (h) for endothelial cells ($CD31^+$) and neural cells ($TUJ1^+$). Representative images from three mice are shown. Anagen induction was performed by hair depilation using hair plucking. Scale bar, 30 μm. Data are shown as means ± SD.

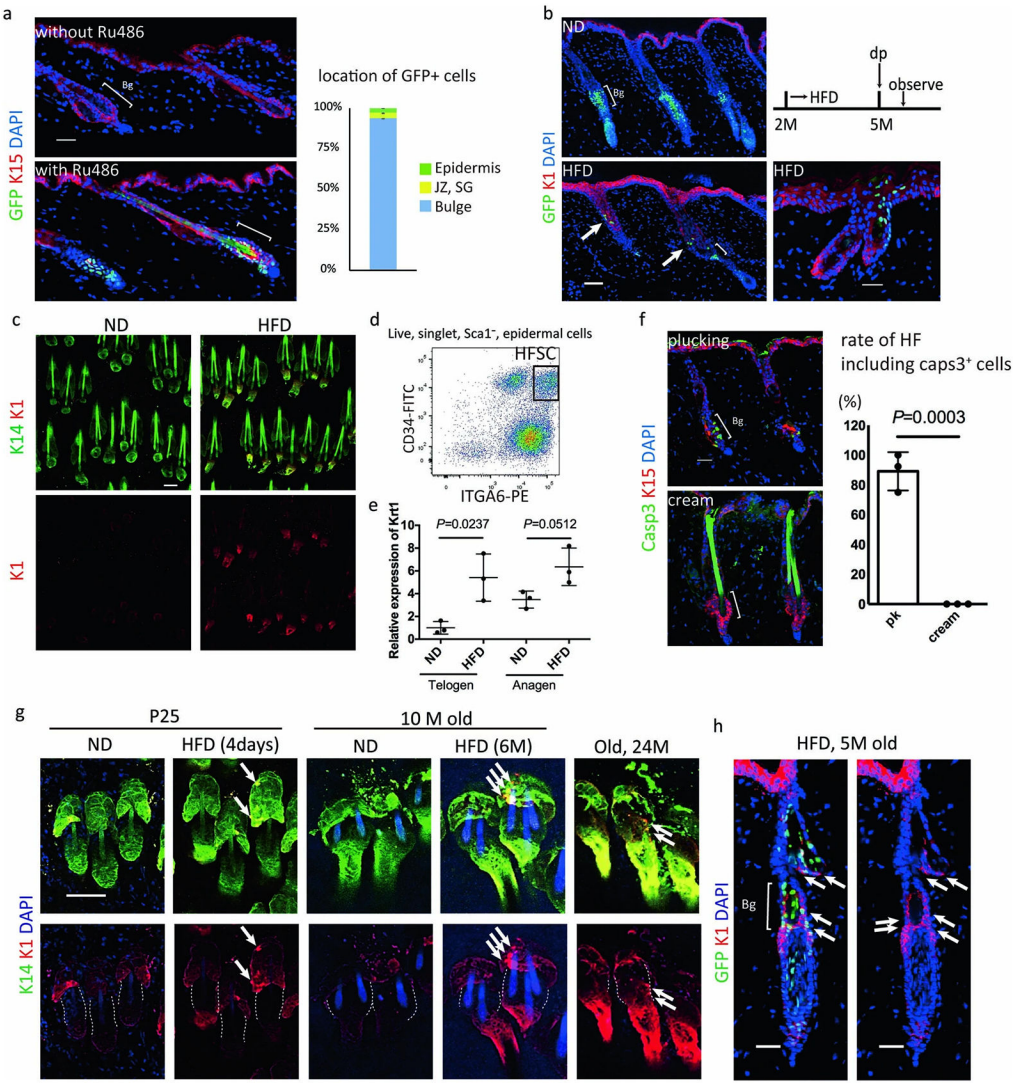

Extended Data Fig. 3 |. HFSCs prematurely commit to epidermal differentiation by HFD-feeding.

a. The location of GFP-positive cells in *K15CrePR:Rosa-H2BGFP* mice after recombination (n=2). *K15CrePR:Rosa-H2BGFP* mice were treated or not treated with RU486 and the locations of GFP-positive cells were counted in RU486-treated mice. Bg, bulge. JZ, junctional zone; SG, sebaceous gland. **b**. Representative immunostaining for GFP and the suprabasal marker K1 from three mice. Some GFP^+ cells, which had been HFSCs at the timing of RU486 treatment, expressed K1 when they moved up to the epidermis. Anagen induction was performed by hair depilation using hair plucking. Scale bar, 30 μm. **c**, Representative whole mount staining for K14 and K1 from three mice. K1 expression was higher in anagen hair follicles of HFD-fed mice than in anagen hair follicles of ND-fed

mice. Scale bar, 60 μm. **d**, FACS analysis of dorsal skin; the $CD34^{high}ITGA6^{high}SCA1^{-}$ population was used as HFSCs for qPCR, microarray analyses and ATAC-sec analysis. **e**, qPCR analysis for *K1* in HFSCs from ND- or HFD-fed mice. n= 4 mice, two-tailed unpaired t-test. Data are shown as means ± SD. **f**, Immunostaining for activated CASP3, a marker for apoptosis, and K15 for dorsal skin with hair plucking or hair removal cream (n=3 mice, two-tailed unpaired t-test). **g**, Whole mount staining of physiological anagen hair follicles (without any experimental treatment to induce anagen) for K1 and K14. Scale bar, 60 μm. Images are representative from p25 mice (n=3), 10M (n=2) or 24M old mice (n=1). Dotted lines show bulge regions. **h**, Representative cross section staining of anagen hair follicles from three HFD-fed *K15crePR:Rosa-H2B-GFP* mice for K1 and GFP. Anagen induction was performed by hair depilation using hair plucking. Scale bar, 50 μm. Arrows indicate ectopic expression of K1 (g,h).

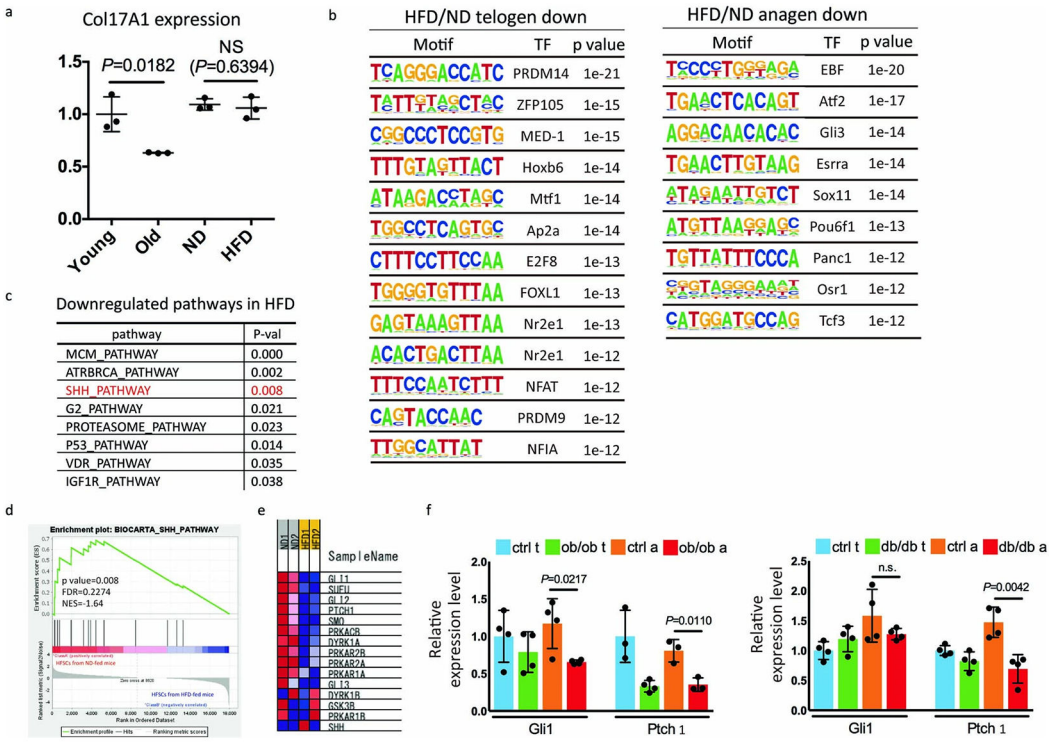

Extended Data Fig. 4 |. Shh signaling is inhibited specifically in HFSCs of HFD-fed mice. **a**, *Col17a1* mRNA expression levels in telogen HFSCs between young, old, ND-fed or HFD-fed mice without depilation (3-months feeding, n=3, two-tailed unpaired t-test, data are shown as means ± SD) derived from microarray data. **b**, Motif analysis of ATAC-seq data. Binomial p-values are shown. **c-e**, RNA-seq analysis for anagen HFSCs from 6-old HFD-fed (4 months HFD) and ND-fed mice (n=2). **c**, Downregulated pathways in anagen HFSCs of HFD-fed mice were analyzed with GSEA by choosing c2.cp.biocarta.v7.2 (curated gene sets) as the gene set correlation. All pathways with GSEA p values <0.05 were shown. **d**, Enrichment plot for the Shh pathway biocarta gene set. **e**, Heatmap of the biocarta Shh pathway gene set core signature represented as Blue-Pink O' Gram in the space of the analyzed gene set. **f**, qPCR analysis using HFSCs of 7-week-old *ob/ob* or *db/db* mice

for *Gli1* and *Ptch1* (n=4, two-tailed unpaired t-test. Data are shown as means ± SD). Ctrl t, control telogen; *obob* t; *ob/ob* mice telogen; Ctrl a, control anagen; *obob* a, *ob/ob* mice anagen; *dbdb* t, *db/db* mice telogen; *dbdb* a, *db/db* mice anagen.

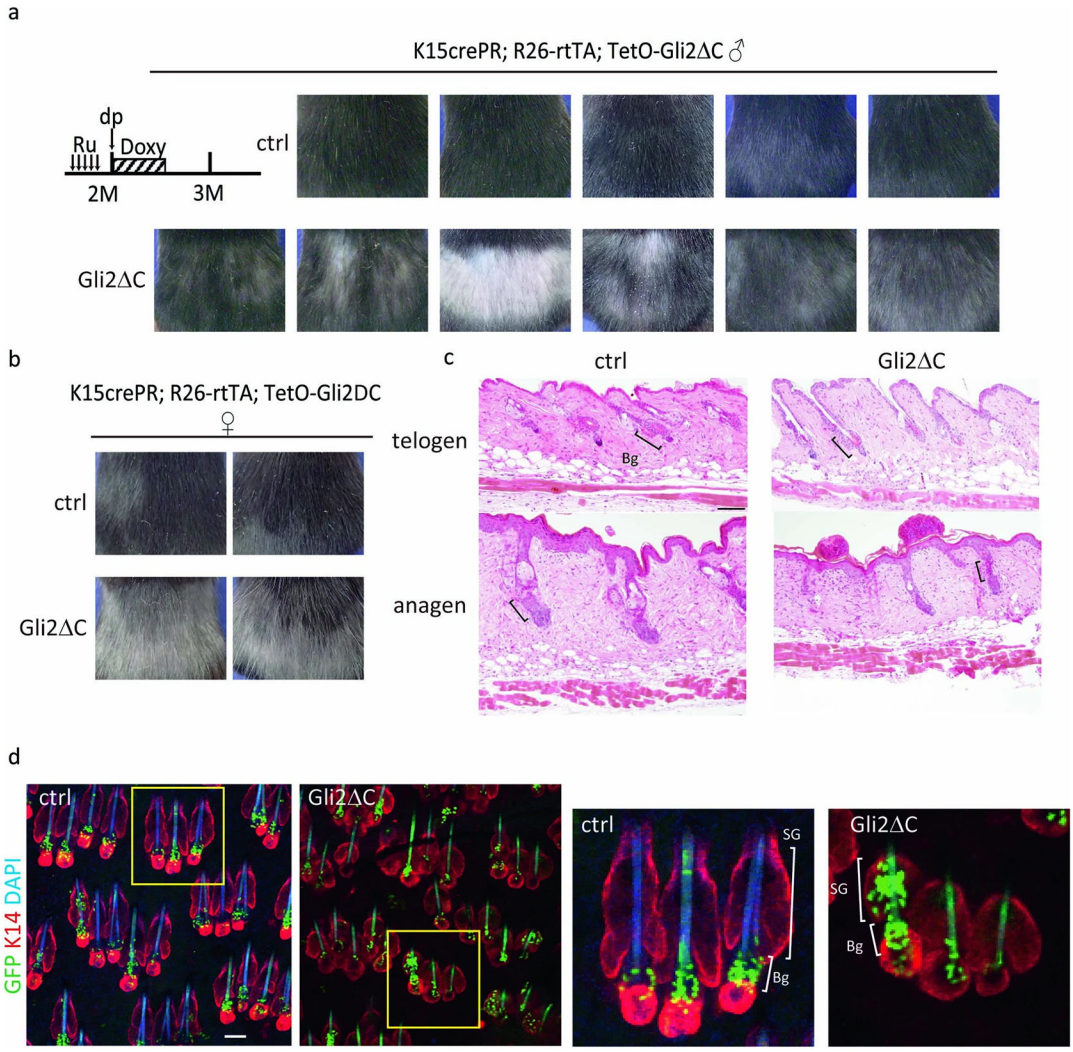

Extended Data Fig. 5 |. Shh inhibition causes hair loss after one hair cycle.

a, Study design and all images of male *Gli2ΔC* mice (control, n=5; *Gli2ΔC*, n=6.). **b**, Images of female *Gli2ΔC* mice (n=2). **c**, Representative HE staining of the dorsal skin from two control or *Gli2ΔC* mice. Bg, bulge. Scale bar, 100 μm. **d**, Representative images of whole mount staining of one *K15crePR; Rosa-H2BEGFP* (ctrl) mice or one *K15crePR; Rosa-rtTA; TetO-Gli2ΔC; Rosa-H2BEGFP* mice 5 days after hair depilation. Ru486 was treated 5 times in 7-week-old mice and Dox treatment was started in 8-week-old mice simultaneously with hair cycle induction by a hair depilation cream. Bg, bulge. Scale bar, 60 μm.

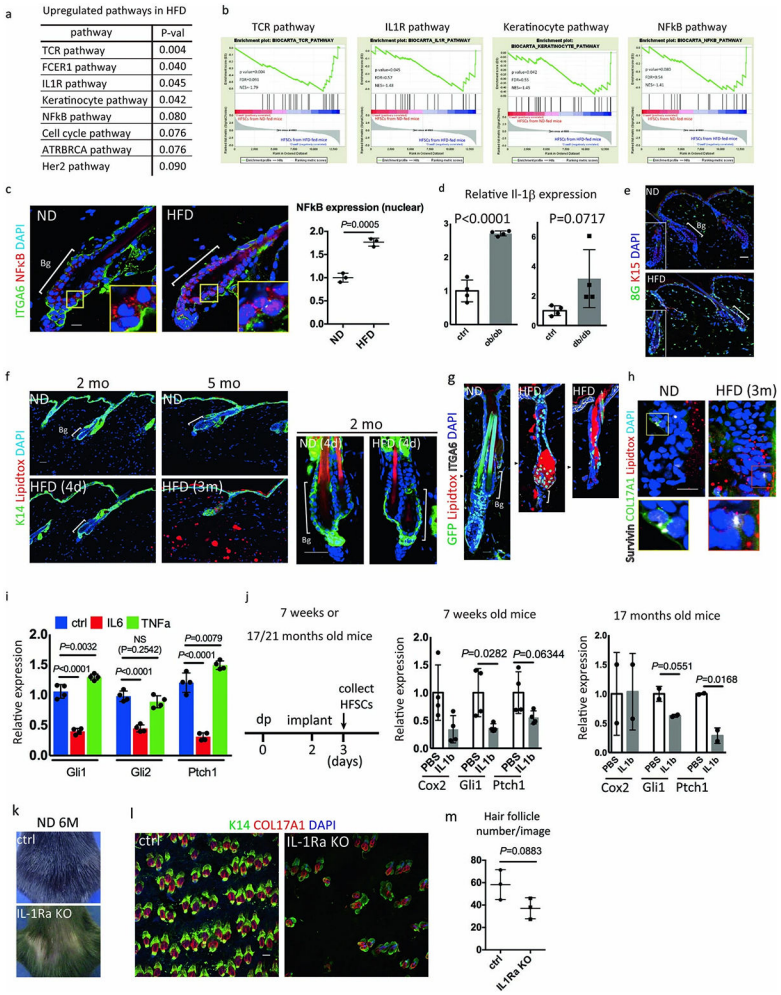

Extended Data Fig. 6 | Intrafollicular inflammatory milieu in HFSCs of HFD-fed mice coordinately inhibits the Shh pathway and promotes the epidermal commitment of HFSCs. **a**, Upregulated pathways in telogen HFSCs of HFD-fed mice (n=3) were analyzed with GSEA by choosing C2 (curated gene sets) as the gene set correlation. All pathways with GSEA p value <0.1 were shown. **b**, GSEA profiles of telogen HFSCs of HFD-fed mice (n=3) compared with ND-fed mice. **c**, Immunostaining of NFκB and ITGA6. The relative intensity of NFκB translocation was calculated in the nuclei of HFSCs in 6 month old mice fed a HFD for 4 months. (n=3, two-tailed unpaired t-test). Scale bar, 10 μm. Bg, bulge. **d**, qPCR analysis for *IL-1β* using whole skin cells of 7-week-old *ob/ob* or *db/db* mice (n=4, two-tailed unpaired t-test). **e**, Representative images of 8-Oxoguanine (8G) and K15 staining of skin after 3 months of a ND or a HFD from three mice. Bg, bulge, **f**, Representative images of neutral lipid staining by lipidtox in telogen HFSCs of 2 month old or 5 month old mice from three mice. mo, month old. Bg, bulge. **g**, Representative images of neutral lipid staining of anagen HFSCs of 6 month old K15crePR; RosaH2BGFP mice fed a ND or a HFD from three mice. **h**, Immunostaining of Lipidtox, survivin and COL17A1 in hair follicle bulge and the germ of anagen day 3. Representative images from three mice are shown. Five month old mice were depilated to induce anagen by plucking. **i**, qPCR analysis of Gli1, Gli2 and Ptch1 were performed after treatment of mouse neonatal skin with IL6

or TNFα (n=4, one-way ANOVA followed by two-tailed Dunnett's test. Data are shown as means ± SD). **j**, Local administration of recombinant IL-1β activates IL-1R signaling and inhibits Shh signaling especially in aged mice. An atelocollagen sponge impregnated with 1 μg IL-1β or PBS was implanted subcutaneously and qPCR analysis was conducted 1 day after treatment in HFSCs. n=4 or n=2 for 7 weeks or 17 months old mice, respectively. two-tailed unpaired t-test. See methods for details. **k**, Representative images of 6-month old *IL-1Ra* KO mice. **l**, Representative whole mount staining of skin from three Ctrl or *IL-1Ra* KO mice. Scale bar, 60 μm. **m**, Hair follicle numbers of 6-month old Ctrl or *IL-1Ra* KO mice (n=3, two-tailed unpaired t-test). Data are shown as means ± SD; exact P values are provided in the Source Data.

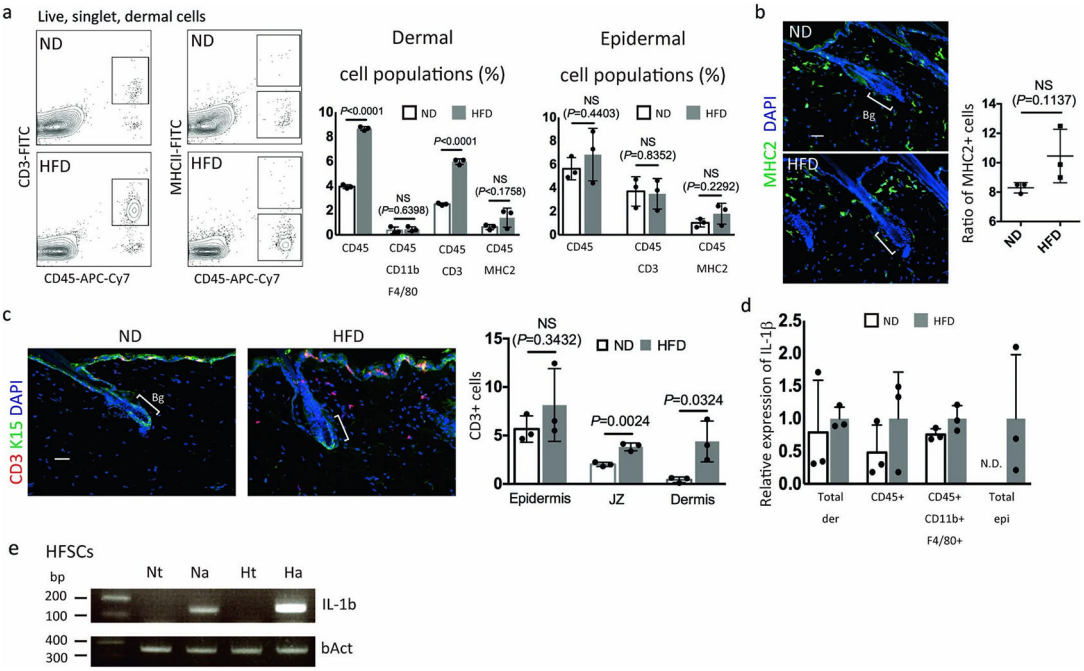

Extended Data Fig. 7 |. Low grade inflammatory milieu of HFD-fed mice stimulates IL-1β signaling in HFSCs.

a, Ratio of total immune cells ($CD45^+$), macrophages ($CD45^+$ $CD11b^+$ $F4/80^+$), T cells ($CD45^+$ $CD3^+$) and $MHC2^+$ cells ($CD45^+$ $MHC2^+$) in the dermis analyzed by FACS for 6 month old mice fed a ND or a HFD (n=3 mice, two-tailed unpaired t-test; exact P values are provided in the Source Data). **b, c**, Immunostaining for MHC2 (b) and CD3 (c) (n=3, two-tailed unpaired t-test) of 6 month old mice fed a ND or a HFD. Bg, bulge. JZ=junctional zone. Scale bars, 30 μm. **d**, qPCR analysis of *IL-1β* in the indicated populations (n=3). Data are shown as means ± SD. N.D. not detected. **e**, qPCR analysis of *IL-1β* in anagen HFSCs from ND-fed or HFD-fed mice. Representative results from four mice are shown. Nt, normal diet telogen; Ht, high fat diet telogen; Na, normal diet anagen; Ha, high fat diet anagen.

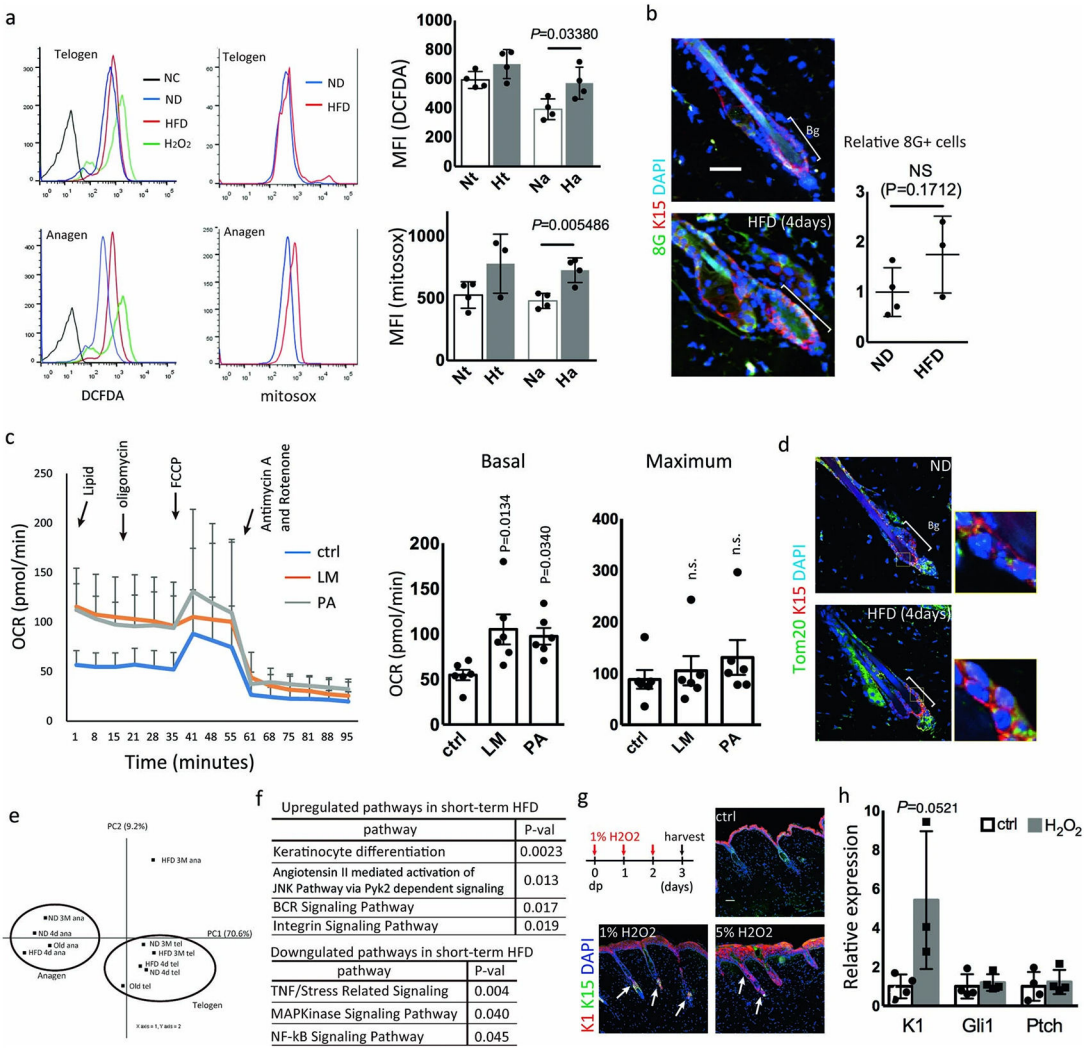

Extended Data Fig. 8 |. Short-term HFD feeding promotes epidermal commitment of HFSCs through the generation of ROS

a, Total intracellular contents of ROS or mitochondrial superoxide production were analyzed using DCFDA and MitoSOX in telogen or anagen HFSCs. 7-week-old mice were fed a ND or a HFD and their dorsal skins were harvested 4 days later (n=4). **b**, 8G staining of skins from ND-fed or HFD-fed mice (n=3, two-tailed unpaired t-test). Bg, bulge. Scale bar, 30 μm. **c**, Oxygen consumption rate (OCR) of total epidermis was measured with lipid mixture or palmitate and the sequential injection of oligomycin, FCCP and rotenone/antimycin. Basal and maximum OCR levels are shown in the graph. LM, lipid mixture. PA, palmitic acid. (n=6, one-way ANOVA followed by two-tailed Dunnett's test. Data are shown as means ± SD). **d**, Immunostaining for Tom20, a mitochondria marker, in hair follicles of 8 week old mice with or without short-term exposure to HFD. Representative images from two mice are shown. Bg, bulge. **e**, PCA analysis of HFSCs after short-term (4 days) or long-term (3 months) treatment with a HFD. **f**, BioCarta pathway enrichment analysis by DAVID was performed using anagen HFSCs of short-term (4 days) treatment with HFD (fold change≥2.0 or <0.5, n=1). **g**, Immunostaining showed that three days of treatment with

1% H_2O_2 or one treatment with 5% H_2O_2 of mouse dorsal skin increased the expression of K1 in anagen HFSCs. **h**, qPCR showed that three days treatment of H_2O_2 increased the expression of *K1* (n=3, two-tailed unpaired t-test) but not Gli1 and Ptch1 in anagen HFSCs. Anagen induction was performed by hair depilation using hair plucking. Data are shown as means ± SD.

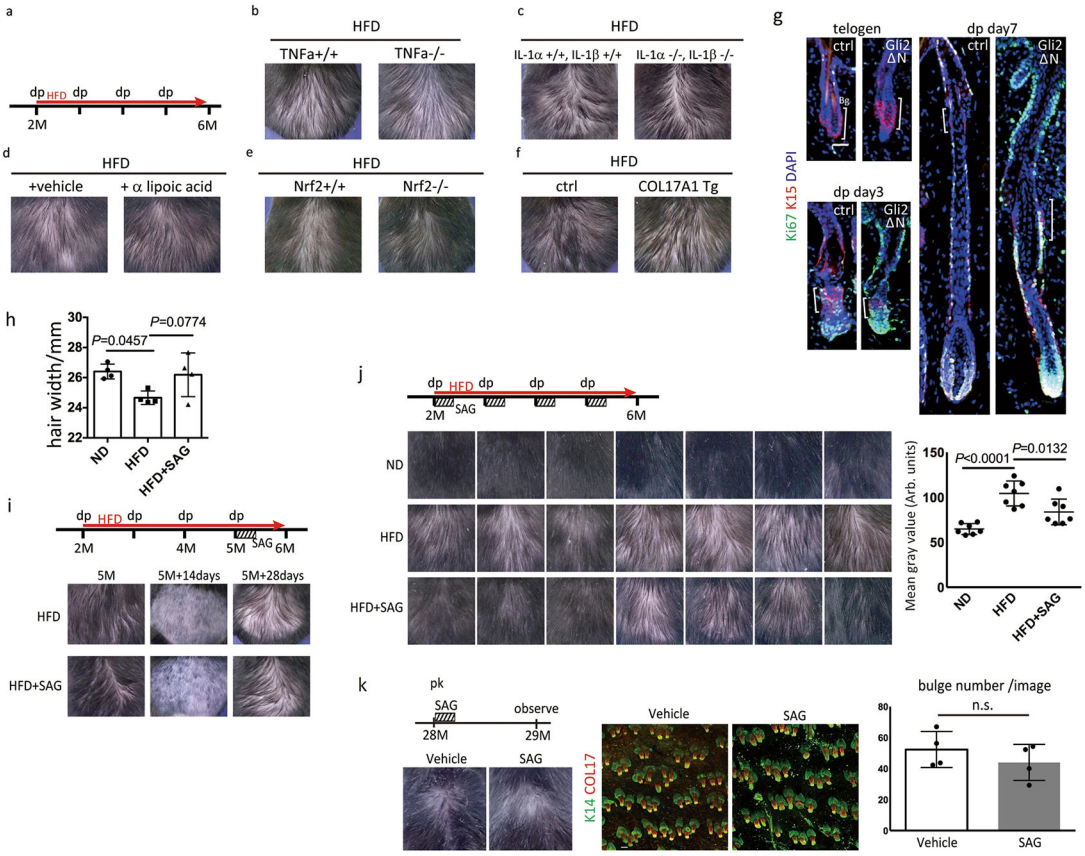

Extended Data Fig. 9 |. Shh signal activation partially rescues HFD-induced hair thinning

a, Experimental design for the experimental procedure. **b, c**, Representative images of *TNFα* KO (n=3) and *IL-1α IL-1β* dKO mice (n=3). **d**, Representative images of HFD-fed mice treated with α–lipoic acid (n=4, see methods). **e**, Representative images of HFD-fed *Nrf2* KO mice (n=3). **f**, Representative images of HFD-fed *COL17A1* Tg mice (Tg, n=4; Ctrl, n=3). **g**, Ki67 staining of *Gli2ΔN* mice. Three days after onset of the hair cycle, the number of proliferating HFSCs of *Gli2ΔN* mice was higher than that of control mice. Anagen induction was performed by hair depilation using hair plucking. Bg, bulge. Scale bar, 30 μm. **h**, Hair width of zigzag hairs in ND-fed, HFD-fed or SAG-treated HFD-fed mice (n=4, one-way ANOVA followed by two-tailed Tukey's test. Data are shown as means ± SD). **i**, One-time treatment with SAG after three months did not rescue the HFD-induced hair loss (n=3). **j**, Treatment with SAG every week after hair depilation rescued the HFD-induced hair loss (n=7, one-way ANOVA followed by two-tailed Tukey's test; exact P values are provided in the Source Data). **k**, Treatment of aged mice with SAG for one week did

not rescued the age-associated hair loss (n=4, two-tailed unpaired t-test. Data are shown as means ± SD).

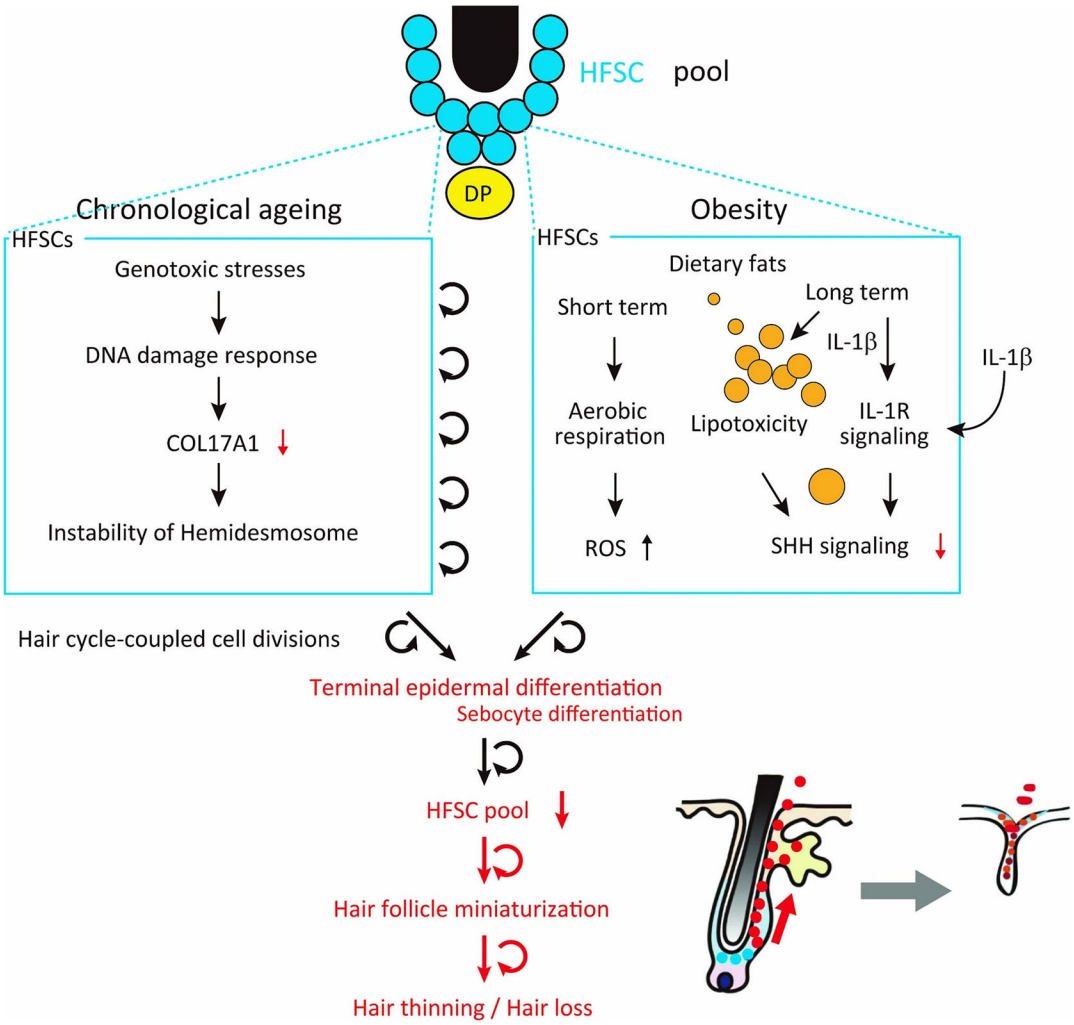

Extended Data Fig. 10 |. Similarities and differences between ageing-induced and obesity-induced hair loss.

Chronological ageing and obesity induces/accelerates hair follicle miniaturization through stem cell depletion that is based on distinct molecular mechanisms. Age-associated repetition of hair cycles causes sustained DNA damage response in HFSCs to reduce their expression of COL17A1, resulting in hemidesmosomal instability which further causes the repetition of atypical stem cell divisions that induce the epidermal differentiation of HFSCs and eventually detach HFSCs from the basement membrane. In sharp contrast, short-term exposure of HFSCs to a HFD causes the accumulation of ROS and long-term exposure causes lipid droplets in HFSCs, activates IL-1R signaling and inhibits Shh signaling, which induces epidermal and sebocyte differentiation and elimination of lipid-laden HFSCs upon hair cycle-coupled activation. In both cases, those aberrant fate changes occur in a small population of HFSCs upon their activation at early anagen, thereby diminishing the pool of HFSCs in those particular follicles and causing the resultant hair follicle miniaturization and

hair thinning in a stepwise manner. Because the skin contains a densely arranged hair follicle bulge (niche) that contains abundant HFSC pools and the expression of the hair thinning phenotype appears with a time delay via the long duration of the hair cycle, HFSC depletion proceeds in a latent manner and manifests the hair thinning/loss phenotype only after several rounds of hair cycles.

Supplementary Material

Refer to Web version on PubMed Central for supplementary material.

Acknowledgements

We thank R. Yajima, H. Katagiri, I. Manabe, S. Wakana and Y. Nabeshima for technical support, and DASS Manuscript for editing. E.K.N. is supported by an AMED Project for Elucidating and Controlling Mechanisms of Ageing and Longevity (JP17gm5010002 - JP21gm5010002), Scientific Research on Innovative Areas “Stem Cell Aging and Disease” (26115003) and by Aderans co ltd. H. Morinaga is supported by a JSPS Grant-in-Aid for Young Scientists (B) (17K15663). A.A.D is supported by NIH grant (R01 AR045973) and Cancer Center Support grant (P30 CA046592).

Data availability

Microarray data were deposited in the GEO public database (accession no. GSE131958). RNA-seq data were deposited in the GEO public database (accession no. GSE169173). All ATAC data were deposited in the DDBJ database (accession no. DRA008515). DAVID web-accessible tool is available at https://david.ncifcrf.gov/tools.jsp. GSEA is available at https://www.gsea-msigdb.org/gsea/index.jsp. TIGRMeV is available at http://mev.tm4.org.

References

1. Novak JSS, Baksh SC & Fuchs E Dietary interventions as regulators of stem cell behavior in homeostasis and disease. Genes Dev 35, 199–211, doi:10.1101/gad.346973.120 (2021). [PubMed: 33526586]
2. Matsumura H et al. Hair follicle aging is driven by transepidermal elimination of stem cells via COL17A1 proteolysis. Science (New York, N.Y.) 351, aad4395, doi:10.1126/science.aad4395 (2016).
3. Calle EE, Rodriguez C, Walker-Thurmond K & Thun MJ Overweight, obesity, and mortality from cancer in a prospectively studied cohort of U.S. adults. N Engl J Med 348, 1625–1638, doi:10.1056/NEJMoa021423 (2003). [PubMed: 12711737]
4. Sakaue S et al. Trans-biobank analysis with 676,000 individuals elucidates the association of polygenic risk scores of complex traits with human lifespan. Nat Med 26, 542–548, doi:10.1038/s41591-020-0785-8 (2020). [PubMed: 32251405]
5. Aune D et al. BMI and all cause mortality: systematic review and non-linear dose-response meta-analysis of 230 cohort studies with 3.74 million deaths among 30.3 million participants. BMJ 353, i2156, doi:10.1136/bmj.i2156 (2016). [PubMed: 27146380]
6. Ambrosi TH et al. Adipocyte Accumulation in the Bone Marrow during Obesity and Aging Impairs Stem Cell-Based Hematopoietic and Bone Regeneration. Cell stem cell 20, 771–784.e776, doi:10.1016/j.stem.2017.02.009 (2017). [PubMed: 28330582]
7. Beyaz S et al. High-fat diet enhances stemness and tumorigenicity of intestinal progenitors. Nature 531, 53–58, doi:10.1038/nature17173 (2016). [PubMed: 26935695]
8. Inomata K et al. Genotoxic stress abrogates renewal of melanocyte stem cells by triggering their differentiation. Cell 137, 1088–1099, doi:10.1016/j.cell.2009.03.037 (2009). [PubMed: 19524511]

9. Oh J, Lee YD & Wagers AJ Stem cell aging: mechanisms, regulators and therapeutic opportunities. Nat Med 20, 870–880, doi:10.1038/nm.3651 (2014). [PubMed: 25100532]
10. Flach J et al. Replication stress is a potent driver of functional decline in ageing haematopoietic stem cells. Nature 512, 198–202, doi:10.1038/nature13619 (2014). [PubMed: 25079315]
11. Hiroyuki Matsumura, N. L, Daisuke Nanba, Shizuko Ichinose, Aki Takada, Sotaro Kurata, Hironobu Morinaga, Yasuaki Mohri, Adèle De Arcangelis, Shigeo Ohno & Emi K. Nishimura Distinct types of stem cell divisions determine organ regeneration and aging in hair follicles. nature aging, doi:10.1038/s43587-021-00033-7 (2021).
12. Matilainen V, Koskela P & Keinänen-Kiukaanniemi S Early androgenetic alopecia as a marker of insulin resistance. The Lancet 356, 1165–1166, doi:10.1016/s0140-6736(00)02763-x (2000).
13. Driskell RR et al. Distinct fibroblast lineages determine dermal architecture in skin development and repair. Nature 504, 277–281, doi:10.1038/nature12783 (2013). [PubMed: 24336287]
14. Salzer MC et al. Identity Noise and Adipogenic Traits Characterize Dermal Fibroblast Aging. Cell, doi:10.1016/j.cell.2018.10.012 (2018).
15. Chen CC, Plikus MV, Tang PC, Widelitz RB & Chuong CM The Modulatable Stem Cell Niche: Tissue Interactions during Hair and Feather Follicle Regeneration. J Mol Biol 428, 1423–1440, doi:10.1016/j.jmb.2015.07.009 (2016). [PubMed: 26196442]
16. Festa E et al. Adipocyte lineage cells contribute to the skin stem cell niche to drive hair cycling. Cell 146, 761–771, doi:10.1016/j.cell.2011.07.019 (2011). [PubMed: 21884937]
17. Rompolas P & Greco V Stem cell dynamics in the hair follicle niche. Semin Cell Dev Biol 25-26, 34–42, doi:10.1016/j.semcdb.2013.12.005 (2014). [PubMed: 24361866]
18. Nakajima T et al. Roles of MED1 in quiescence of hair follicle stem cells and maintenance of normal hair cycling. J Invest Dermatol 133, 354–360, doi:10.1038/jid.2012.293 (2013). [PubMed: 22931914]
19. Greco V et al. A two-step mechanism for stem cell activation during hair regeneration. Cell stem cell 4, 155–169, doi:10.1016/j.stem.2008.12.009 (2009). [PubMed: 19200804]
20. Xing L et al. Alopecia areata is driven by cytotoxic T lymphocytes and is reversed by JAK inhibition. Nat Med 20, 1043–1049, doi:10.1038/nm.3645 (2014). [PubMed: 25129481]
21. St-Jacques B*†, D. HR, Karavanova I†, Botchkarev VA‡, Li J§, & Danielian PS*, M. JA, Lewis PM*, Paus R‡ and McMahon AP*. Sonic hedgehog signaling is essential for hair development. Curr Biol 8 (1998).
22. Ouspenskaia T, Matos I, Mertz AF, Fiore VF & Fuchs E WNT-SHH Antagonism Specifies and Expands Stem Cells prior to Niche Formation. Cell 164, 156–169, doi:10.1016/j.cell.2015.11.058 (2016). [PubMed: 26771489]
23. Hsu YC, Li L & Fuchs E Transit-amplifying cells orchestrate stem cell activity and tissue regeneration. Cell 157, 935–949, doi:10.1016/j.cell.2014.02.057 (2014). [PubMed: 24813615]
24. Ermilov AN et al. Maintenance of Taste Organs Is Strictly Dependent on Epithelial Hedgehog/GLI Signaling. PLoS Genet 12, e1006442, doi:10.1371/journal.pgen.1006442 (2016). [PubMed: 27893742]
25. Furukawa S et al. Increased oxidative stress in obesity and its impact on metabolic syndrome. J Clin Invest 114, 1752–1761, doi:10.1172/JCI21625 (2004). [PubMed: 15599400]
26. Lichti U, Anders J & Yuspa SH Isolation and short-term culture of primary keratinocytes, hair follicle populations and dermal cells from newborn mice and keratinocytes from adult mice for in vitro analysis and for grafting to immunodeficient mice. Nat Protoc 3, 799–810, doi:10.1038/nprot.2008.50 (2008). [PubMed: 18451788]
27. Wang Y et al. Interleukin-1beta induces blood-brain barrier disruption by downregulating Sonic hedgehog in astrocytes. PLoS One 9, e110024, doi:10.1371/journal.pone.0110024 (2014). [PubMed: 25313834]
28. Horai R et al. Production of mice deficient in genes for interleukin (IL)-1alpha, IL-1beta, IL-1alpha/beta, and IL-1 receptor antagonist shows that IL-1beta is crucial in turpentine-induced fever development and glucocorticoid secretion. The Journal of experimental medicine 187, 1463–1475 (1998). [PubMed: 9565638]

29. Tanaka Y et al. NF-E2-related factor 2 inhibits lipid accumulation and oxidative stress in mice fed a high-fat diet. J Pharmacol Exp Ther 325, 655–664, doi:10.1124/jpet.107.135822 (2008). [PubMed: 18281592]

30. Grachtchouk M et al. Basal cell carcinomas in mice arise from hair follicle stem cells and multiple epithelial progenitor populations. J Clin Invest 121, 1768–1781, doi:10.1172/JCI46307 (2011). [PubMed: 21519145]

31. Ito M et al. Stem cells in the hair follicle bulge contribute to wound repair but not to homeostasis of the epidermis. Nat Med 11, 1351–1354, doi:10.1038/nm1328 (2005). [PubMed: 16288281]

32. Taniyama Y et al. Beneficial effect of intracoronary verapamil on microvascular and myocardial salvage in patients with acute myocardial infarction. J Am Coll Cardiol 30, 1193–1199 (1997). [PubMed: 9350914]

33. Itoh K et al. An Nrf2/small Maf heterodimer mediates the induction of phase II detoxifying enzyme genes through antioxidant response elements. Biochem Biophys Res Commun 236, 313–322 (1997). [PubMed: 9240432]

34. Nishie W et al. Humanization of autoantigen. Nat Med 13, 378–383, doi:10.1038/nm1496 (2007). [PubMed: 17322897]

35. Yang RL, Li W, Shi YH & Le GW Lipoic acid prevents high-fat diet-induced dyslipidemia and oxidative stress: a microarray analysis. Nutrition 24, 582–588, doi:10.1016/j.nut.2008.02.002 (2008). [PubMed: 18367378]

36. Fujiwara H et al. The basement membrane of hair follicle stem cells is a muscle cell niche. Cell 144, 577–589, doi:10.1016/j.cell.2011.01.014 (2011). [PubMed: 21335239]

37. Jensen KB, Driskell RR & Watt FM Assaying proliferation and differentiation capacity of stem cells using disaggregated adult mouse epidermis. Nat Protoc 5, 898–911, doi:10.1038/nprot.2010.39 (2010). [PubMed: 20431535]

38. Ba X & Boldogh I 8-Oxoguanine DNA glycosylase 1: Beyond repair of the oxidatively modified base lesions. Redox Biol 14, 669–678, doi:10.1016/j.redox.2017.11.008 (2018). [PubMed: 29175754]

39. Solanas G et al. Aged Stem Cells Reprogram Their Daily Rhythmic Functions to Adapt to Stress. Cell 170, 678–692 e620, doi:10.1016/j.cell.2017.07.035 (2017). [PubMed: 28802040]

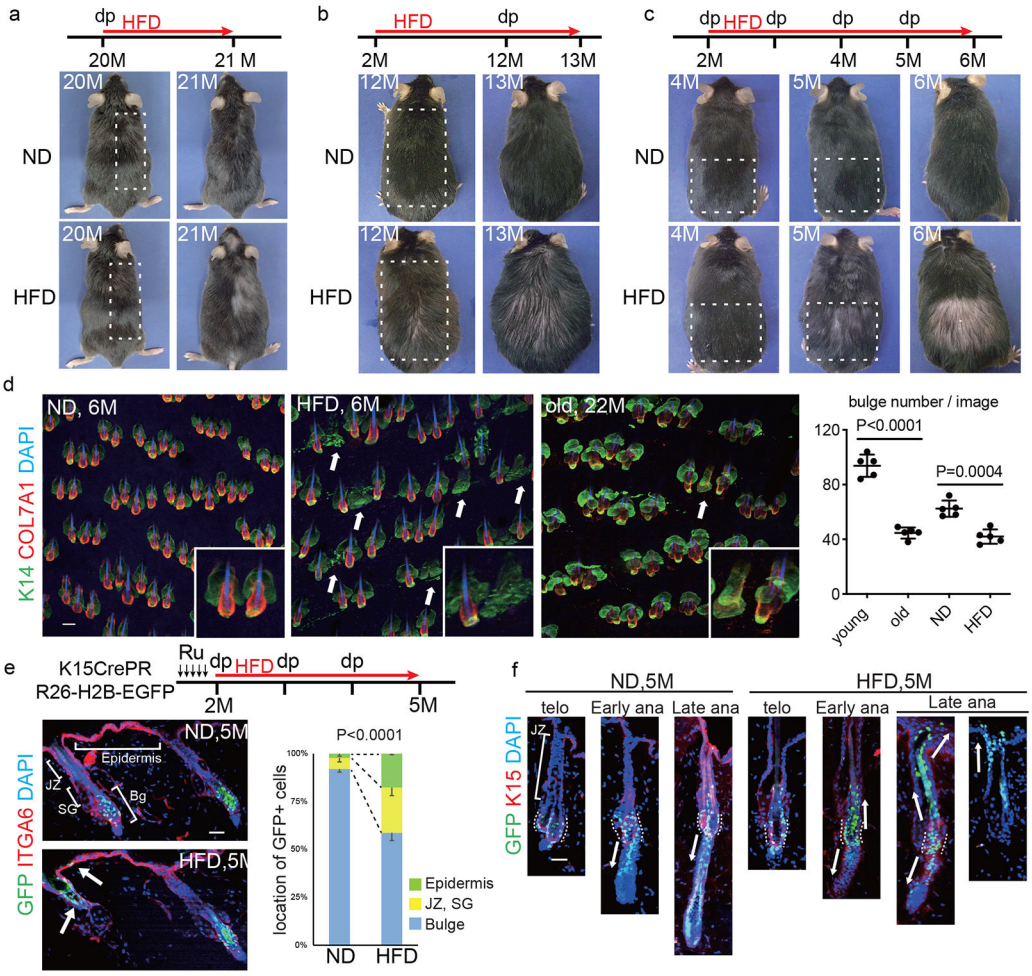

Fig. 1 |. Obesity accelerates hair loss through fate switching and depletion of hair follicle stem cells (HFSCs).

a,b, Representative images of normal-diet (ND)-fed or high-fat-diet (HFD)-fed mice. Treatment with the HFD started at 20 months old (**a**, n=4) or at 2 months old (**b**, n=8). Hair depilation (dp) was conducted at the indicated times, **c**, Representative images of HFD-fed mice whose dorsal hair was depilated in the indicated area every month (n>24). **d**, Representative whole mount images and hair follicle numbers of 6-month old mice (4-month feeding of ND or HFD) with monthly hair depilation or of 22-month old mice. Arrows indicate follicles without a detectable HFSC-containing bulge (n=5, two-tailed unpaired t-test). Scale bar, 60 μm. **e**, Lineage trace of HFSCs in hair follicles of ND- or HFD-fed mice (n=1313 (ND) or 1295 (HFD) GFP^+ cells from 3 mice, two-tailed chi-square test). Ru, Ru486. Bg, bulge. JZ, junctional zone; SG, sebaceous gland. Scale bar, 30 μm. **f**, Lineage trace of HFSCs during the hair cycle. Representative images from four mice are shown. telo, telogen; ana, anagen. Dotted lines show bulge regions and arrows indicate the direction of movement of GFP^+ cells. Anagen induction was performed by hair depilation using hair plucking. Scale bar, 30 μm. Exact P values are provided in the Source Data. Data are shown as means ± SD.

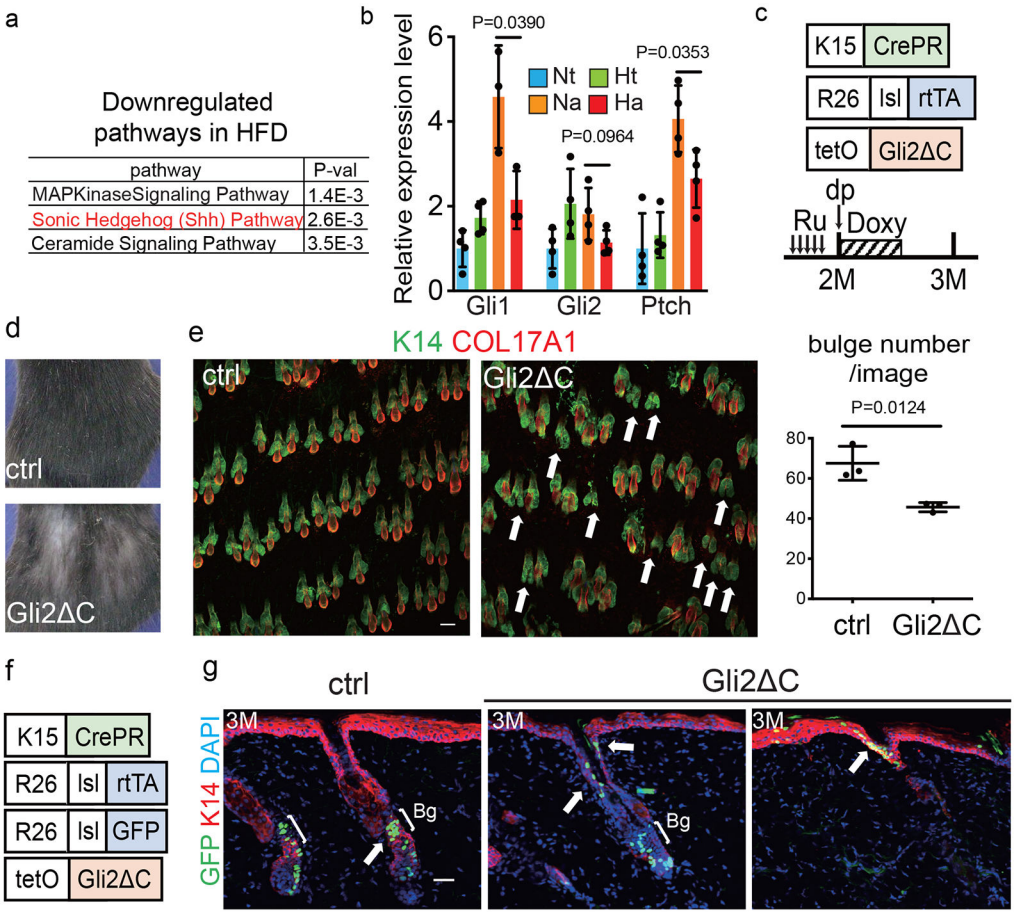

Fig. 2 l. A HFD inhibits the Shh pathway to promote the fate switching of HFSCs toward epidermal differentiation.

a, BioCarta pathway enrichment analysis was performed by DAVID using anagen HFSCs from five-month-old ND- or HFD-fed mice (fold change≤0.5, n=1 from 4 (ND) or 8 (HFD) mice) isolated three days after hair depilation. **b**, qPCR analysis using HFSCs for *Gli1, Gli2* and *Ptch1*, which are related to the Shh pathway (Gli1 of anagen HFSCs, n=3; others, n=4, two-tailed unpaired t-test). Nt, normal diet telogen; Ht, high fat diet telogen; Na, normal diet anagen; Ha, high fat diet anagen. **c**, Schematic of the experimental design for HFSC-specific inhibition of Shh signaling in mice (*Gli2ΔC* mice). Ru, Ru486; Doxy, doxycycline. **d**, Representative images of control and *Gli2ΔC* mice. **e**, Whole mount images and hair follicle number of the dorsal skin of *Gli2ΔC* mice (n=3, two-tailed unpaired t-test). Arrows indicate follicles without bulges. Scale bar, 60 μm. **f,g**, Lineage trace of HFSCs in *Gli2ΔC* mice. Representative images from three mice are shown. Anagen induction was performed by hair depilation using hair plucking. Bg, bulge. Scale bar, 30 μm. Data are shown as means ± SD.

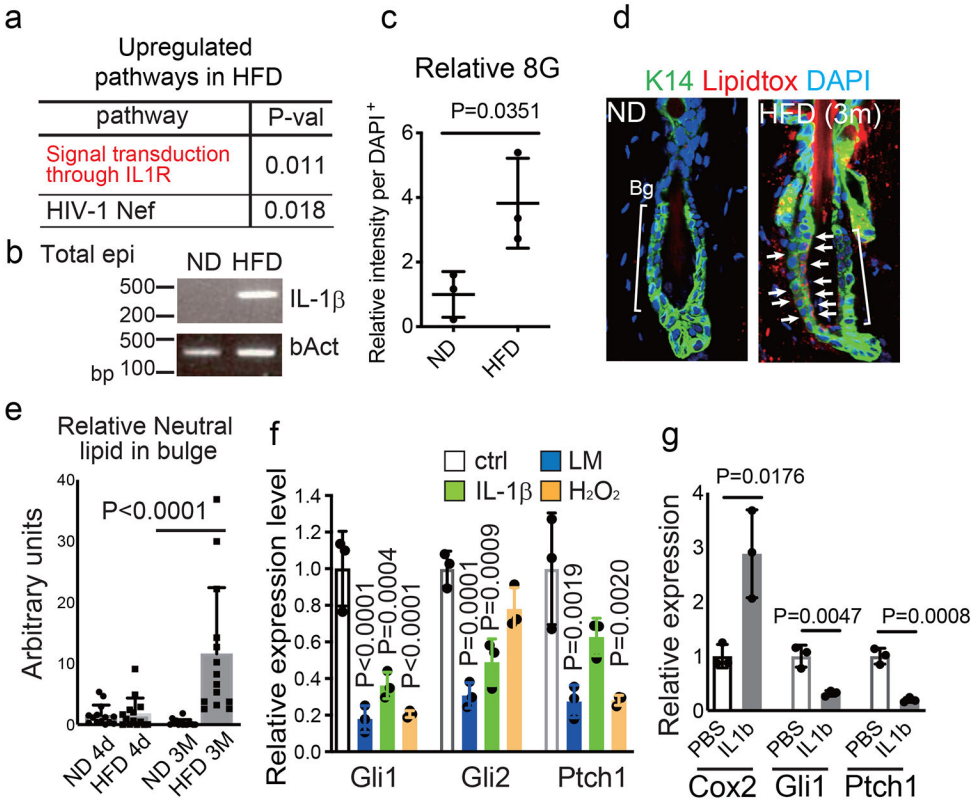

Fig. 3 |. HFD-induced stem cell inflammageing with oxidative stress accelerates HFSC depletion and resultant hair loss through the inhibition of Shh signaling.

a, BioCarta pathway enrichment analysis by DAVID was performed using telogen HFSCs ($p<0.1$, fold change≥2.0, n=3 mice). **b**, qPCR analysis of *IL-1β* in Total epidermis from ND-fed or HFD-fed mice. Representative images from three mice are shown. **c**, 8-Oxoguanine (8G) and K15 staining of skin after 3 months of a ND or a HFD (n=3, two-tailed unpaired t-test). **d, e**, Neutral lipid staining by lipidtox in HFSCs of 5 month old mice fed a HFD for 3 months. Bg, bulge. N, ND. H, HFD. (n=15 hair follicles from 3 mice. two-tailed Mann–Whitney U-test. Data are shown as means ± SD). **f**, qPCR analysis of *Gli1, Gli2* and *Ptch1* in mouse neonatal skin after treatment with the indicated compounds (n=3, one-way ANOVA followed by two-tailed dunnett's test). **g**, qPCR analysis of *Cox2, Gli1* or *Ptch1* after local administration of recombinant IL-1β in anagen HFSCs of 22-month old mice (n=3, two-tailed unpaired t-test). Exact P values are provided in the Source Data. Data are shown as means ± SD.

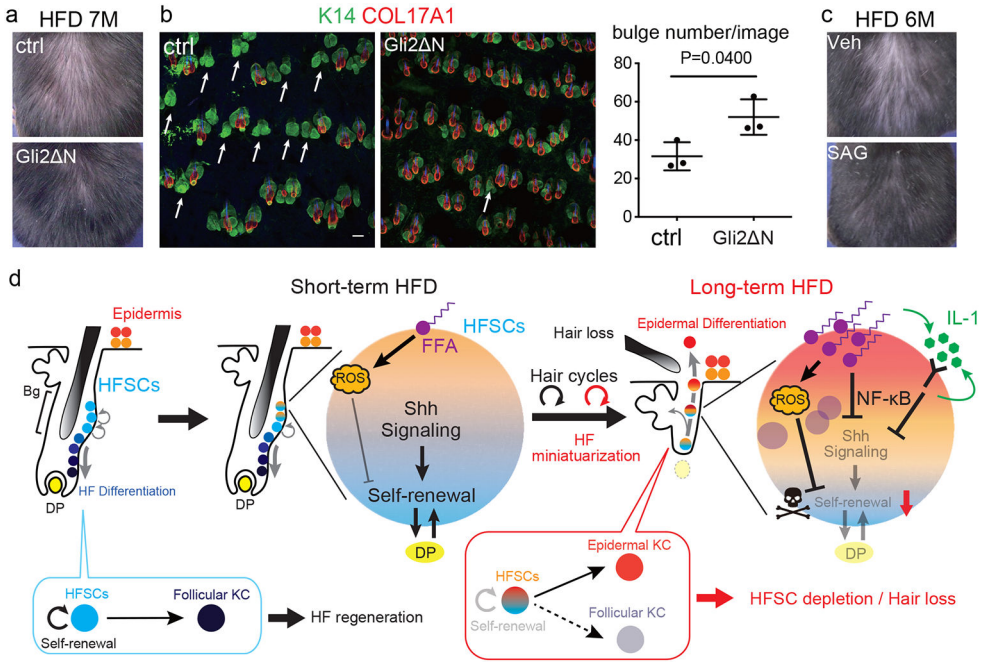

Fig. 4 |. Shh activation in HFSCs prevents HFD-induced hair loss by targeting the converging roots of HFSCs.

a, Representative images of wt and *K19CreER; Rosa-rtTA; TetO-Gli2ΔN* mice after 5 months of a HFD. *Gli2ΔN* mice were treated with tamoxifen at 7 weeks old and with doxycycline for one week after each depilation. **b**, Whole mount imaging of dorsal skin of control and *Gli2ΔN* mice (n=3, two-tailed unpaired t-test). Arrows indicate follicles without HFSC-containing bulges. Scale bar, 60 μm. Data are shown as means ± SD. **c**, Representative images of HFD-fed mice treated with or without SAG, a hedgehog activating reagent, for one week after each depilation (n=7, see Extended Data Fig. 9j). Veh, vehicle. **d**, Schematic of our proposed mechanism of the HFD-induced hair loss. Short-term HFD feeding induces epidermal differentiation program by accumulating ROS via aerobic respiration, yet retains the HFSC pool. Long-term HFD feeding additionally induces NFκB signaling and accumulation of abundant lipid, which causes HFSC depletion and eventual hair loss. Bg, bulge. DP, dermal papilla. FFA, free fatty acids.